The impact of aging on pial arteriolar reactions and cerebrocortical blood flow variations with spreading depolarization

Doctoral Thesis

Puskás Tamás

University of Szeged

Faculty of Medicine, Faculty of Science and Informatics

Department of Medical Physics and Informatics

The impact of aging on pial arteriolar reactions and cerebrocortical

blood flow variations with spreading depolarization

Doctoral Thesis

Puskás Tamás

Supervisor: Dr. Farkas Eszter

Doctoral School of Theoretical Medicine

Szeged, 2020

Table of Contents

List of publications related to the subject of the thesis:

I.   Ákos Menyhárt, Dániel Zölei-Szénási, <u>Tamás Puskás</u>, Péter Makra, Ferenc Bari, Eszter Farkas

Age or ischemia uncouples the blood flow response, tissue acidosis, and direct current potential signature of spreading depolarisation in the rat brain

AMERICAN JOURNAL OF PHYSIOLOGY: HEART AND CIRCULATORY PHYSIOLOGY 313: (2) pp. H328-H337. (2017)

https://doi.org/10.1152/ajpheart.00222.2017

Scimago classification: Medicine/Physiology(medical); Ranking: 22/107 (Q1)

II.   Armand R. Bálint*, <u>Tamás Puskás</u>*, Ákos Menyhárt, Gábor Kozák, Imre Szenti, Zoltán Kónya, Tamás Marek, Ferenc Bari, Eszter Farkas

* These Authors contributed equally to the work.

Aging impairs cerebrovascular reactivity at preserved resting cerebral arteriolar tone and vascular density in the laboratory rat

FRONTIERS IN AGING NEUROSCHIENCE 11 Paper: 301, 12 p. (2019)

https://doi.org/10.3389/fnagi.2019.00301

Scimago classification: Aging; Ranking: 8/34 (Q1)

Abbreviations

2VO: 2-vessel occlusion (transient bilateral common carotid artery occlusion)

aCSF: artificial cerebrospinal fluid

ANOVA: analysis of variance

CBF: cerebral blood flow

CeVD: Cerebrovascular disease

CVD: Cardiovascular disease

DC: direct current

CUDA: Compute Unified Device Architecture

ECoG: electrocorticogram

EU: European Union

GPU: Graphic Processing Unit

IOS: intrinsic optical signal

LASCA: laser speckle contrast analysis

MABP: mean arterial blood pressure

MCT1: monocarboxylic acid transporter 1

NMDA: N-methyl-D-aspartate

NR: neutral red

pHe: extracellular pH

pHi: intracellular pH

ROI: region of interest

ROS: reactive oxygen species

SD: spreading depolarisation

StDev: Standard deviation

1. Introduction

1.1. Importance of Cerebral stroke

The importance of cerebral stroke is underscored by its high incidence, considerable mortality, the structure of the examined population and consequential economic relations. There have been significant improvements in the prevention and risk factor management in the last decades, which led to a reduced disease incidence in Europe. The mortality of cerebrovascular diseases (CeVD) notably declined, as well as the mortality of cardiovascular diseases (CVD). Despite these trends, CeVDs have remained the second leading cause of death, stroke responsible for 9% and 13% of all deaths in man and women in Europe, respectively. On the other hand the increasing prevalence of risk factors for CeVD, such as obesity, diabetes and high blood pressure is predicting an upcoming slow-down in this declining progress of CeVDs.[1,2,3]

In the European Union (EU), nearly 20% of the population is older than 65 years (data of 2018). It is an approximately 2.5%. increase in 10 years across the EU. A similar trend is obvious in Hungary, where the >65 age group represented nearly 19% of the population in 2019 as compared to 16% in 2008[I]. Aging poses an increasing burden on the social service and health care systems, because aging is the most important independent risk factor for chronic degenerative diseases. As such, the incidence of CeVDs is substantially increasing with advancing age[4,5] (*Figure 1*).
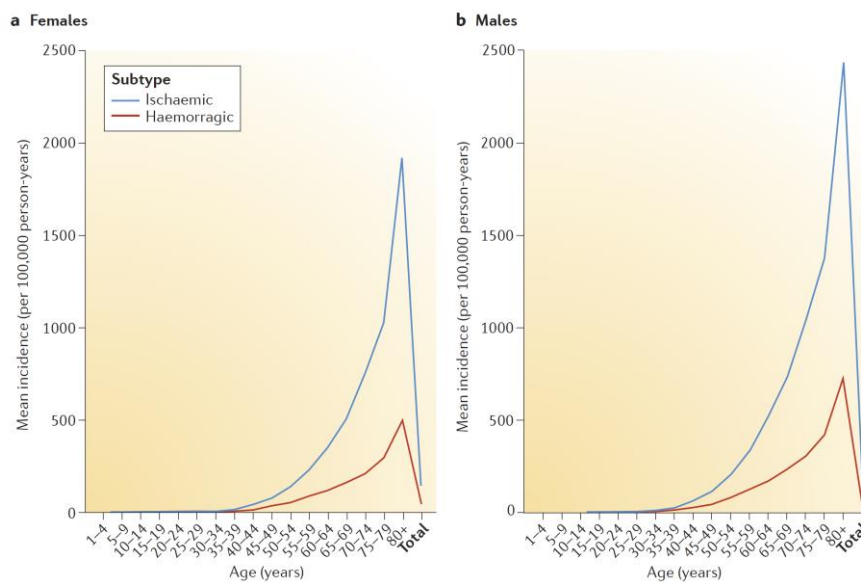

Figure 1. Incidence of ischaemic and haemorragic stroke by age in females and males in Europe.[4]

In 2017 the Stroke Alliance for Europe has launched the Burden of Stroke in Europe overview to establish a coherent and comprehensive overview of stroke care pathway across Europe. Their main goals formulated were the planning of care improvement and standardizing the stroke care across the EU states. It has emphasised the importance of public health intervention of the decision makers (governments of European states and the leaders of EU) with the following realisations: The number of stroke survivors is increasing but parallelly the number of people with disabilities too[4] (*Figure 2*). In the next 20 years the proportion of aged population will dramatically increase. The projections of Burden of Stroke Report indicate in this 20-year long time window a 34% increase in the total number of stroke events in the EU (from 613148 in 2015 to 819771 in 2035). The necessity of country-based monitoring and preparation was urgently advised to avoid overwhelming of national healthcare systems and the families touched by stroke[II].
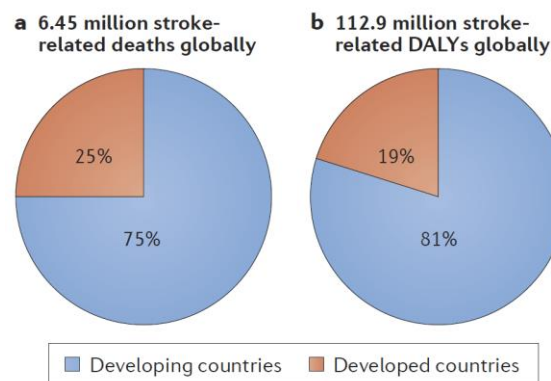
Figure 2. Absolute numbers and proportions of stroke-related deaths and disability-adjusted life years (DALYs) by country development status in 2013.[4]

1.2. Cerebral stroke: mechanism and importance of spreading depolarisation

Two subtypes of stroke are discriminated. A rupture of blood vessels in the brain can cause haemorrhagic stroke. With a much higher incidence - 87% of all cases – the most common type of stroke is ischemic[6]. It is caused by the interruption of the constant cerebral blood flow (CBF). The obstruction of a cerebral artery can block the supply to its distal region. These obstructions can be caused by the narrowing or total blockade of blood vessels (atherosclerosis), or by embolization. Upon the obstruction of a cerebral blood vessel, CBF of the main supplied area drops to 10-25%, <10 ml/100g/min and the tissue will necrotize. It is called the ischemic core region. The tissue embracing the core region called penumbra suffers a CBF reduction down to

30-40%, approximately 15-40 ml/100g/min. The cells in this area are viable but electrophysiologically non-functional. Over the days and weeks subsequent to stroke onset, the core region extends at the expense of the penumbra. The sustained decrease of blood supply maintains a chronic metabolic crisis which culminates in intracellular accumulation of calcium, elevated level of extracellular potassium and intensive glutamate release. These metabolic changes favor the recurrence of an event called spreading depolarisation (SD), which facilitates the expansion of the ischemic core region and predicts worsening neurological outcome[7,8].

Spreading depolarization was described by Leão in 1944 but the mechanisms and its related effects form the focus of intensive research to this day. The role of SDs is fundamental in the pathophysiology of different neurovascular diseases like migraine with aura, ischemic stroke or haemorrhagic stroke. SD corresponds to the near complete breakdown of the resting membrane potential of a critical mass of neurons, which propagates over the cerebral gray matter at a slow rate (2-8 mm/min)[9,10]. This is coupled with a robust but transient suppression of the electrocorticographic activity known as spreading depression of activity. The restoration of the membrane potential requires the mobilization of metabolic resources for the operation of ATP-dependent ion pumps (e.g. the Na^+/K^+ ATP-ase), which need is met by a profound hyperemic cerebral blood flow (CBF) response coupled to SD in otherwise non-compromised tissue[11]. The coupling between SD and local CBF becomes impaired under ischemia, which may create a metabolic supply-demand mismatch, a subsequent energy crisis superimposed on prevailing ischemia, and facilitated tissue injury[12].

There are four characteristic components of SD-related hyperemia: first an initial brief hypoperfusion, second a marked, transient peak hyperemia, third a less obvious late hyperemia and fourth a sustained hypoperfusion (it is also called post-SD oligemia)[11]. In normoxic conditions the hyperemic component is the most pronounced in the young brain, while it becomes shorter and negligible during ischemia, where the hypoperfusion is the dominating component[13–16]. In addition to the SD-related CBF variation, the hemodynamic response propagating with SD is obvious at the level of the pial and penetrating arterioles[9,10,17–19].

The metabolic crisis during SD results in an accumulation of lactate in the affected area, which leads to an acidic pH shift. SD-related acidosis shows additive characteristic to ischemia related acidosis, where a broader cortical area is affected[20]. Tissue pH has long been proposed to

control CBF and was shown to mediate functional hyperemia associated with seizure activity[21]. The higher amplitude of tissue acidosis with SD was strongly correlated with the higher amplitude of the SD-related hyperemia in young adult rats[20].

1.3. Physiological alterations of the aged brain

The structural and functional integrity of the cerebral microvascular system is essential for optimal neural function. It has been long documented that the cerebral arteriolar tree, capillary bed, and venous circulation may undergo (mal)adaptational structural rearrangement with aging[22–26]. Cerebral blood flow (CBF) at rest appears to be lower in the aging brain[22,23,26], and the reactivity of the cerebral microvasculature to neuronal activation or hypercapnic challenge becomes less efficient, partly because of an increased burden of oxidative stress.[27–31] Weakening neural control, particularly the loss of cholinergic innervation of cortical microvessels from the basal forebrain, or inadequate noradrenergic signaling from the locus coeruleus may also account for failing vasoregulation at old age[22,32–34]. Further, the neurovascular unit and blood-brain barrier function has been found to be subject to molecular and biochemical alterations with aging[35–37]. Collectively, these age-related modifications of the cerebral microvascular system have been implicated in cognitive impairment[22,38,39] and worse outcomes after ischemic stroke with increasing age[40–44].

1.4. Spreading depolarisation related alterations and aging

The regulation of the CBF response to SD has been a target of intensive research, but its nature and mediators have not been unequivocally identified. First, the hyperemic component of the CBF response was perceived as reactive hyperemia predominantly driven by metabovascular coupling[45]. This view was later revised, and the increased perfusion in response to SD was assumed to be functional hyperemia mediated by neurovascular coupling to support the restoration of resting membrane potential. Sufficient nutrient supply afforded by hyperemia is converted to ATP to be used by energy-dependent ion pumps[11]. However, the hyperemic component of the CBF response to SD becomes insufficient in brain tissue being challenged by ongoing ischemia[12,13,46], and may be compromised further by aging[16,47,48]. The delayed or obstructed delivery of nutrients postpones or altogether aborts repolarization after SD[12]. Importantly, the increasing cumulative duration of recurrent SD events or irreversible

depolarization from a single event may prove lethal to the tissue[12,49], because high intracellular Ca^{2+} content sustained with SD, accumulating partly through NMDA receptors and voltage-gated Ca^{2+} channels, leads to excitotoxic damage[46,50,51].

In a recent study[20], we found, in the cerebral cortex of young adult rats, that the higher amplitude of tissue acidosis with SD strongly correlated with the higher amplitude of the SD-related hyperemia, supporting the view of a potential metabolic coupling. This observation has prompted us to hypothesize that the intensity of depolarization must be proportional to the magnitude of the subsequent tissue acidosis, which, in turn, should drive the evolution of the ensuing hyperemia with SD. Indeed, tissue pH has long been proposed to control CBF[52,53] and was shown to mediate functional hyperemia associated with seizure activity[21].

With aging, SDs propagating over the ischemic cerebral cortex appear to be increasingly more harmful, as evidenced by the enlarged surface of cortical tissue involved in prolonged depolarization[54]. Repolarization may be delayed in the aging cortex because recovery from SD-related acidosis is considerably hampered by age[20] and the SD-related hyperemia becomes insufficient and often seriously impaired (i.e., spreading ischemia)[16,17,20,54]. All of these together have been considered to indicate or promote the conversion of the ischemic penumbra to the irreversibly damaged core region[20,46], a pathophysiological process accelerated in the aged brain[18,40,47,54]. Despite the age-related weakening of hyperemia in response to SD, there is no evidence that the intensity of the underlying depolarization would proportionally be smaller. This raises the assumption that age weakens the coupling between SD and the associated hyperemia. Such a hypothesis is reasonable, since age has been shown to impair neurovascular coupling with somatosensory stimulation, probably due to the increased production of NADPH oxidase-derived ROS in the neurovascular domain[28,39]. Similarly, neurovascular coupling was found dysfunctional immediately or days after cerebral ischemia onset, as indicated by failing functional hyperemia in response to preserved neuronal activity corresponding to somatosensory stimulation[19].

1.5. Experimental optical neuroimaging, as a tool to study SD

Traditionally, SD events are recorded with a single or an array of microelectrodes. In addition, ion translocations or the metabolic condition of the tissue may be followed with ion-sensitive microelectrodes. Although the use of electrodes offers excellent temporal resolution of the

signal, the investigation of the spatial evolution of SD and the associated metabolic changes requires the application of imaging techniques that offer high spatial resolution.

The spatial resolution of the voltage signal indicative of SD was first realized with the application of a voltage sensitive dye, whose fluorescence intensity increased with decreasing transmembrane potential[55].

In the service of our research efforts to tackle the coupling between SD and the associated CBF response, we have developed an experimental, multi-modal wide-field optical imaging system that offers an appropriate spatio-temporal resolution for studying SD[56]. The combination of two of the synchronous modalities, laser-speckle contrast analysis (LASCA) and intrinsic optical signal (IOS) imaging at green light illumination offers a unique opportunity to examine CBF changes synchronous with variations of pial arteriolar caliber, and pial arteriolar architecture[56,57]. Finally, we established tissue pH imaging in our preparations with the use Neutral Red (NR), a vital dye that indicates changes of intracellular pH (pHi). We adapted NR imaging to monitor pHi changes with SD in the rat cerebral cortex, and combined it with LASCA-based CBF imaging to directly relate tissue pH changes to CBF variations[20].

1.6. Goals

Based on the above, we sought to evaluate how ischemia or age would influence the perceived association between SD, CBF and tissue acidosis.

Accordingly, our goals were:

- to evaluate whether the dilation of pial arterioles in response to SD is impaired by aging;
- to investigate whether the density and resting diameter of the pial vascular network might be subject to aging;
- to determine whether the spatial pattern of flow distribution during SD propagation in the cerebral cortex is altered by aging;
- to systematically explore meaningful associations between the kinetics of the typical direct current (DC) potential signature of SD, the related variations in tissue pH, and the hyperemic component of the CBF response.

2. Materials and Methods

2.1. Series 1

2.1.1. Closed cranial window preparation and experimental protocol

The experimental procedures were approved by the National Food Chain Safety and Animal Health Directorate of Csongrád County, Hungary. The procedures conformed to the guidelines of the Scientific Commitee of Animal Experimentation of the Hungarian Academy of Sciences (updated Law and Regulations on Animal Protection: 40/2013. (II. 14.) Gov. Of Hungary), following the EU Directive 2010/63/EU on the protection of animals used for scientific purposes, and reported in compliance with the ARRIVE guidelines.

Young (n=20, 2 month-old) and old (n=18, 18-20 month-old), male, isoflurane-anesthetized (1.1-1.3% isoflurane in N_2O-O_2/7:3), spontaneously breathing Sprague-Dawley rats were used in the main project. The body temperature was maintained between 37.1 °C and 37.3°C with a feedback-controlled heating pad (Homeothermic Blanket System, Harvard Apparatus, Holliston, USA). The mean arterial blood pressure (MABP) was continuously monitored from the cannulated femoral artery (RX104A, TSD104A, Biopac Systems, Inc, Goleta, USA). After a cervical incision, silicone-coated fishing lines were carefully looped around both common carotid arteries as an occluder for the later induction of acute, incomplete, global forebrain ischemia (2-vessel occlusion, 2VO). A closed cranial window (4.5x4.5 mm) was built over the parietal cortex. A ring shape barrier of acrylic dental cement with a perfusion inlet and outlet (aCSF; mM concentrations: 126.6 NaCl, 3 KCl, 1.5 $CaCl_2$, 1.2 $MgCl_2$, 24.5 $NaHCO_3$, 6.7 urea, 3.7 glucose bubbled with 95 % O_2 and 5 % CO_2 to achieve a constant pH of 7.4 perfusion; 25 μm/min) and two glass microcapillaries were mounted around the craniotomy. The first capillary was connected to a syringe pump to inject 1 μl 1 M KCl for SD elicitation (CMA/100, CMA /Microdialysis, Stockholm, Sweden) at the caudo-medial side. The other one, an intra-cortical glass capillary electrode was placed near the opposite, fronto-parietal edge of the craniotomy. The registering of direct current (DC) potentials (reference electrode was placed under the skin of the animal's neck) was needed to confirm the SD occurrence *(Figure 3/C)*. The recording system consisted of a pre-amplifier (NL102G), a differential amplifier (NL106) a filter and conditioner system (NL125, NL530, NeuroLog System, Digitimer Ltd Welwyn Garden City, Hertfordshire, England) and a noise eliminator to eliminate 50 Hz line frequency

noise (HumBug, Quest Scientific Instruments Inc., North Vancouver, Canada). The cranial window was sealed with a glass coverslip.
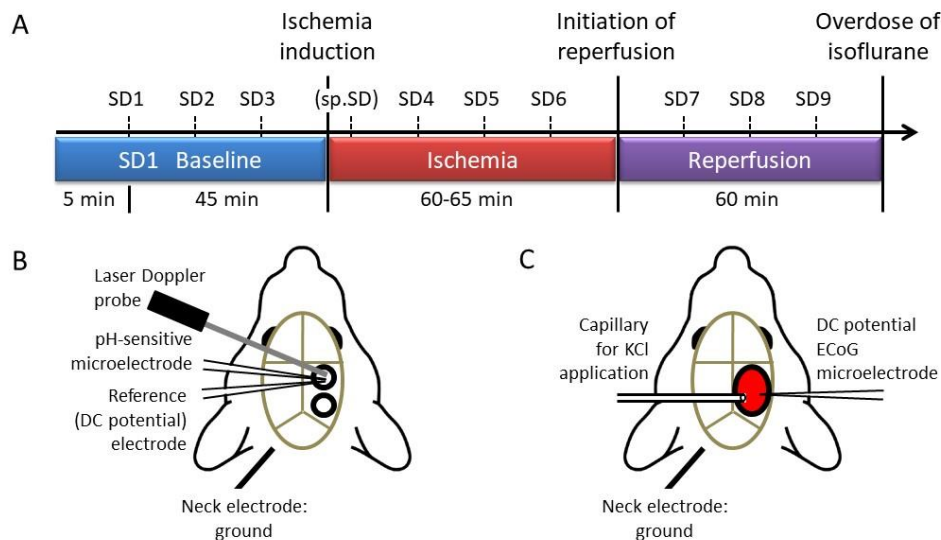

Figure 3. Experimental paradigm and models. **A,** Schematic illustration of the experimental protocol. Numbered spreading depolarization events (e.g. SD1, SD2, … SD9) indicate SDs evoked by 1M KCl application. Spontaneous SD (sp.SD) evolved in some but not all experiments, and is given in brackets due to its inconsistent occurrence. Ischemia and reperfusion were induced by the occlusion and latter release of both common carotid arteries. **B-C,** Experimental preparation for the various data acquisition protocols used. **B,** Conventional electrophysiological setting. Two open cranial windows were created (black circles) over the right parietal cortex. The frontal window served as recording site for data acquisition, and the caudal window was used for SD elicitation by the topical application of 1M KCl. **C,** Preparation for multimodal imaging (Laser speckle contrast analysis). A closed cranial window was built over the parietal (black ellipse filled with red). The cranial window was equipped with a glass capillary to apply 1 µl of 1 M KCl topically to elicit SD (left), and a glass capillary microelectrode to acquire direct current (DC) potential and electrocorticogram (ECoG) (right).

After the surgical procedures, we have collected data over three subsequent phases of the experiments: During the baseline period (50 min), the cerebral perfusion was intact. Next, acute global forebrain ischemia was induced by 2VO (1 hour). Finally, a reperfusion period (1 hour) followed, initiated by the release of the common carotid arteries. The experiments were terminated by the overdose of isoflurane. The data acquisition continued for a few minutes after the termination of the experiments to allow the recording of biological zero. 3 SD-s were elicited with an interval of 15 min (1 µl, 1M KCl) during each phase of the experiments. *(Figure 3/A)*

2.1.2. LASCA and green IOS imaging

The experimental, optical imaging system was developed in our lab. Image acquisition was achieved with two identical monochrome charge-coupled device cameras (Pantera 1M30, DALSA, Gröbenzell, Germany), providing an image resolution of 1024x1024 pixels (pixel size: 3.71 µm). A stereomicroscope (MZ12.5, Leica Microsystems, Wetzlar, Germany) equipped with a 1:1 binocular/video-tube beam splitter allowed the synchronous recording of images with the two cameras (Frame rate: 1/s in each modality). The tissue was excited with a light emitting diode (530 nm peak wavelength, SLS-0304-A, Mightex Systems, Pleasanton, CA, and bandpass filter 3RD, 540-570 nm, Omega Optical, Battleboro, VT, illumination: 100 ms/s). This narrow wavelength, positioned on the isosbetic point of haemoglobin allowed the registration of green intrinsic optical signal (green reflectance or IOS, exposure: 100ms/s). A laser diode (HL6545MG, Thorlabs, Newton, NJ, 120 mW, 660 nm emission wavelength, power supply: LDTC0520, Wavelength Electronics, Bozeman, MT) as an additional light source was used to illuminate the cortical surface (2 ms for illumination, 100 ms for exposure) to generate CBF maps, based on LASCA. Background images were captured in every cycle to eliminate accidental noise by subtraction of background images of the final image squences. The light sources and the exposure of the cameras were controlled with a custom-made program written in LabVIEW environment (National Instruments, Austin, TX). The calculation of CBF maps from the raw speckle images was computed offline in MATLAB (The MathWorks, Natick, MA).

Local changes of signal intensity (IOS and LASCA) were extracted as time series from each modality by placing regions of interests (ROI) of ~70x70 µm on the selected blood vessel-free cerebrocortical parenchyma. The vascular density of the pial surface in the field of view and the diameter changes of pial arterioles as time series were calculated by using the green IOS images. The CBF maps were used for a deeper spatial analysis of spatial CBF distribution, too.

2.1.3. Data processing: pial vascular density and pial arteriolar diameter

An experimental session, according to our experimental paradigm (see in Chapter 2., *Figure 3*) was ~170 minutes long. A picture (size: of 2 megabytes) was taken in every second in each modality, adding up to a final size of about 20 gigabytes for each recorded modality in each experiment. To process this high amount of data, the high memory capacity and the GPU

(Graphic Processing Unit) based CUDA (Compute Unified Device Architecture) - parallel programming technology were essential. Twenty-five custom made functions were created for proper data processing in Matlab. All of them were shaped to minimize computational time. The most complex one – which needed the highest computational capacity and programming efforts – was created to eliminate movement artefacts (*Figure 4*).

Green IOS images provide a sharp contrast between pial vessels (high green light absorption by hemoglobin) and the cortical parenchyma (low green light absorption by the nervous tissue), which enables reliable automated edge detection to serve the estimation of pial vascular density and changes in pial arteriolar diameter[56].

The correction of tissue swelling-related movement artefacts was achieved with a 2D cross correlation-based algorithm on green reflectance images. Detection of tissue movements around the ROIs (150x150 pixels, embodies ROI surface) was used picture by picture during analysis of vascular reactions. The correction was slightly modified by the spatial perfusion analysis, where 1200 random position ROI-like squares (45x45 pixels) were defined and an average movement vector was calculated for every image based on the positions of the first picture *(Figure 4)*.

First, the pial vascular density was calculated in the green IOS images. The first green IOS frame was smoothed (15 x 15 pixel square box filter), rotated by 0, 11.25, … 90 degrees in all experiments. The edges were detected along the horizontal and vertical axes. Vessels were considered if local minima and local maxima of the first spatial derivative corresponding to the putative edges were detected within 100 pixels. Vessels, which were found in all rotated images were included. In a second approach, the smoothed images were segmented into vessel—no vessel areas by simple thresholding. Threshold intensity was manually determined for each animal. For a third approach, vessel contours were detected by applying a Canny edge detection on raw images. Finally, the outcome of these three approaches were merged and manually adjusted, if necessary. Vascular density was estimated in an 1800×1800 μm area centered on the field of view.

In order to measure changes in arteriolar diameter, we refined a method previously validated in our lab[56]. Three arterioles in their order of branching were selected in the field of view for the analysis. A rectangular region of interest (ROI) was manually positioned on the selected

arteriolar segments. A segment of the largest caliber arteriole entering the field of view from the frontal direction was taken before its first branching (first order vessel). Next, its first branch arteriole (second order vessel), and an order lower branch (third order vessel) were analyzed (Fig. 3A). The analysis script written in a MatLab environment first detected and corrected tissue swelling-related movement artifacts by a 2D cross-correlation based algorithm, and calculated vessel diameter in each image in a sequence based on Canny edge detection. *(Figure 6/A)*

2.1.4. Data processing: evaluation of local cerebral blood flow

CBF recordings obtained by LASCA[58] were expressed relative to baseline by using the average CBF value of the first 240 s of baseline (100%) and the recorded biological zero obtained after terminating each experiment (0%) as reference points. Local changes of CBF were first assessed by conventional single point analysis, by positioning small ROIs (size ~19 × 19 pixels) in the CBF maps, at increasing distances from the site of SD elicitation, to extract changes in signal intensity with time[20,59](*Figure 4/A,B*)

Next, spatial CBF distribution over the cortical parenchyma was estimated in CBF maps, according to previously established principles[54,57]. Swelling-related movement artifacts were eliminated as described above for green IOS images, to serve the spatial match of the parenchymal areas in subsequent images. The relevant parenchymal area was determined by excluding the pial vascular network and bone edges visible in the field of view (black mask in Fig. 4C). The relative area occupied by pixels corresponding to given perfusion ranges (by an increment of 10 % between 0 % and 300 % - i.e. 0-10, 11-20, 21-30 % etc…) was determined in a MatLab environment.
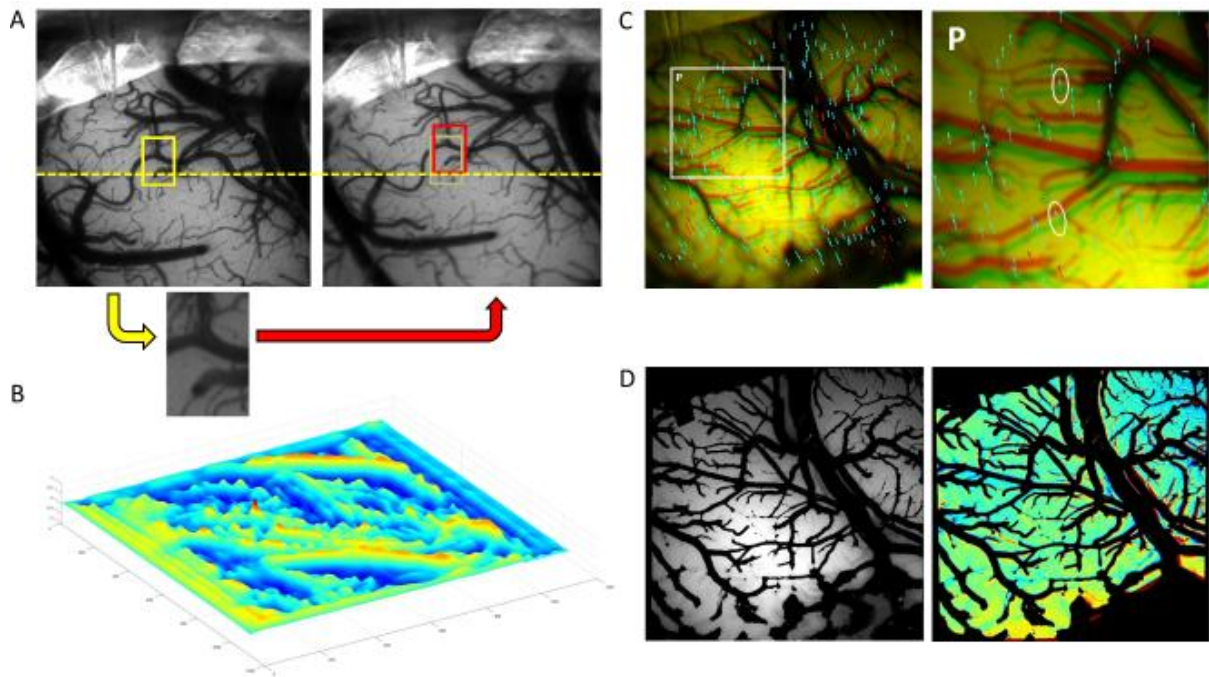
Figure 4. Correction of tissue swelling related movement artefacts and masking of bone and vessel covered surfaces for spatial CBF analysis. **A.** Illustration of the movement detection by the vascular analysis. A small area around the ROI was selected as a template on the first picture (yellow rectangle, yellow striped line is a reference for the original position). The most similar pattern (red rectangle) was searched in each following picture to estimate a vector of displacement. **B.** The highest correlation coefficient (Red spike on the surface) on a 2D cross correlogram shows the displacement of the actual template area. **C.** The movement detection by the spatial analysis was achieved with the tracking of 1200 random template area. The average of these vectors was applied as a main displacement vector. The first (green) and the examined (red) pictures are coloured and merged for representation purposes. The two ellipses on the magnified area show easily detectable corresponding vessel segments. **D.** After the correction procedures the vessel covered and bone surfaces were masked and the CBF maps were calculated on the parenchymal surface. The representative picture from the baseline period shows just negligible deviations in CBF (green - unchanged, blue – slightly lower, yellow – slightly higher perfusion).

2.1.5. Data presentation and statistical analysis

The software SPSS was used for statistical analysis (IBM SPSS Statistics for Windows, Version 22.0, IBM Corp.). Data are provided as mean ± standard deviation of the mean (StDev). When the impact of age was evaluated for a single variable (e.g., pial vascular density), an independent samples T-test was used. For other data sets, a one-way or two-way analysis of variance (ANOVA), or a repeated-measures model was used, dictated by the type of data set. Levels of significance were defined as $*p < 0.05$ and $**p < 0.01$.

2.2. Series 2

2.2.1. Preparation for elctrophysiological recording and experimental protocol

The experimental protocol given under 2.1.1. was replicated in an additional set of animals (n=17) using electrophysiological data acquisition. Two craniotomies were drilled on the

parietal bone. The dura was carefully incised and the surface was regularly irrigated with aCSF. The caudal window served the elicitation site for SDs with the topical application of 1 M KCl.

A laser doppler probe (Probe 403 connected to PeriFlux 5000; Perimed AB, Sweden), a pH-sensitive micro electrode (ion-sensitive electrodes were constructed according to Voipio and Kaila[60]) and a reference DC potential electrode were positioned in the rostral cranial window. An Ag/AgCl neck electrode served as a common ground *(Figure 3/B)*.The two electrodes were connected to a custom-made dual-channel high input impedance electrometer (AD549LH, Analog Devices, Norwood, MA, USA) via Ag/AgCl leads. A differential amplifier (NL834) subtracted the signal of reference electrode from the signal of pH-sensitive electrode. The signal was amplified with an analog signal isolator amplifier (NL820) and forwarded to an analog-to-digital converter (MP 150, Biopac Systems, Inc; filter: NL125; conditioner: NL530; Sampling rate: 1 kHz). The preparations were isolated in a Faraday cage. Electric signals and digitized laser doppler flowmetry data were displayed live, and stored with the software AcqKnowledge 4.2.0 (Biopac Systems Inc., USA). Extracellular pH (pHe) changes were expressed in mV to be translated into pH units offline, using least squares linear regression[20].

2.2.2. Data processing and statistics: correlation analysis between variables

Experiments were selected for data analysis based on the quality of the recordings: experiments in which all synchronous variables (i.e., DC potential, tissue pH, and CBF) were of high quality (i.e., devoid of noise or artefact during SD events) to allow reliable quantitation were processed. The duration and relative amplitude of the negative DC potential shift indicative of SD, of the related acidosis, and of hyperaemia were measured. For group comparisons, data are given as means ± standard deviation (StDev) and were statistically tested by a two-way ANOVA paradigm (factors: phase of experiments and age of animals) of SPSS software (IBM SPSS Statistics for Windows, version 22.0, IBM Corp.). Correlation analysis between variables was achieved by a two-tailed Pearson correlation test run in the same statistical software. Levels of significance were determined and labelled as in the figures $*p < 0.05$ and $**p < 0.01$.

3. Results

3.1. Series 1

3.1.1. Vascular architecture

Despite the anticipation that cerebral microvascular rarefaction should take place with aging in rodents[61 42], in this study approximately half of the cortical surface was covered by pial vessels equally in both young and old rats *(Figure 5)*.
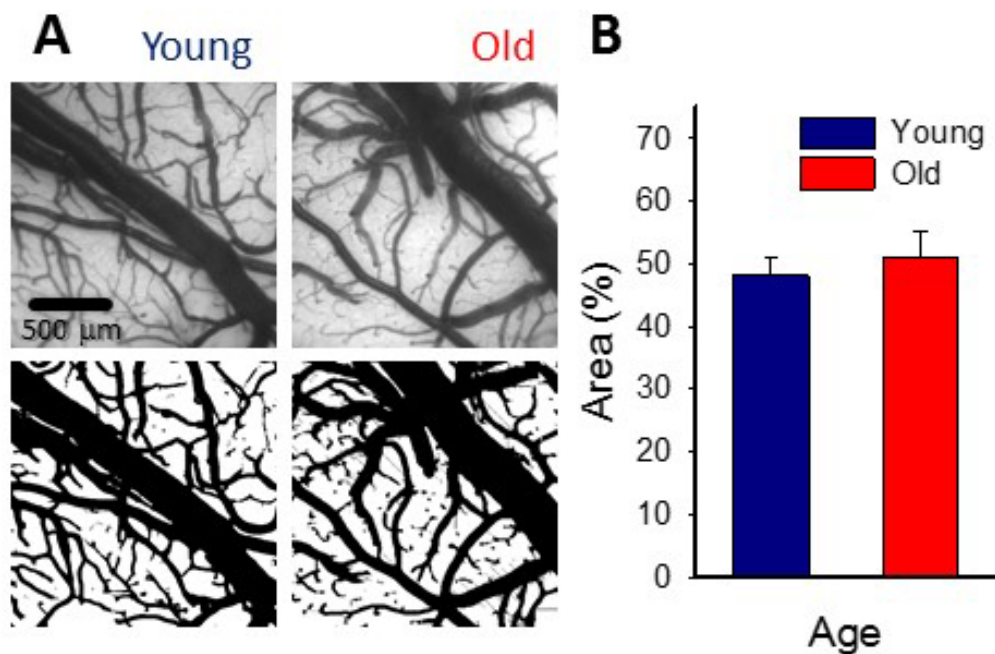

Figure 5. Pial vascular density. **A**, Representative images (top) of the pial surface of a young and an old preparation at green light illumination (orientation: medial to the top, rostral to the right). The relative area covered by vessels was calculated in computed images (bottom). **B**, Vascular density was expressed as the area covered by the pial vascular network relative to the full image size. Data are given as mean±stdev (n=11/10, young/old). An independent samples T-test was used to statistically evaluate age-related differences (p<0.112).

3.1.2. Changes of pial arteriolar diameter and CBF: Event-free segments of the recording

Resting pial arteriolar diameter taken before the elicitation of the first SD obviously decreased along the branching order significantly (83±16, 51±18 and 31±9 µm, 1st, 2nd and 3rd order vessels in the young group *F=20,951, p<0.0001), but was similar in the two age groups (84±16, 54±8 and 34±5 µm, 1st, 2nd and 3rd order vessels in the old group) *(Figure 6/B)*.
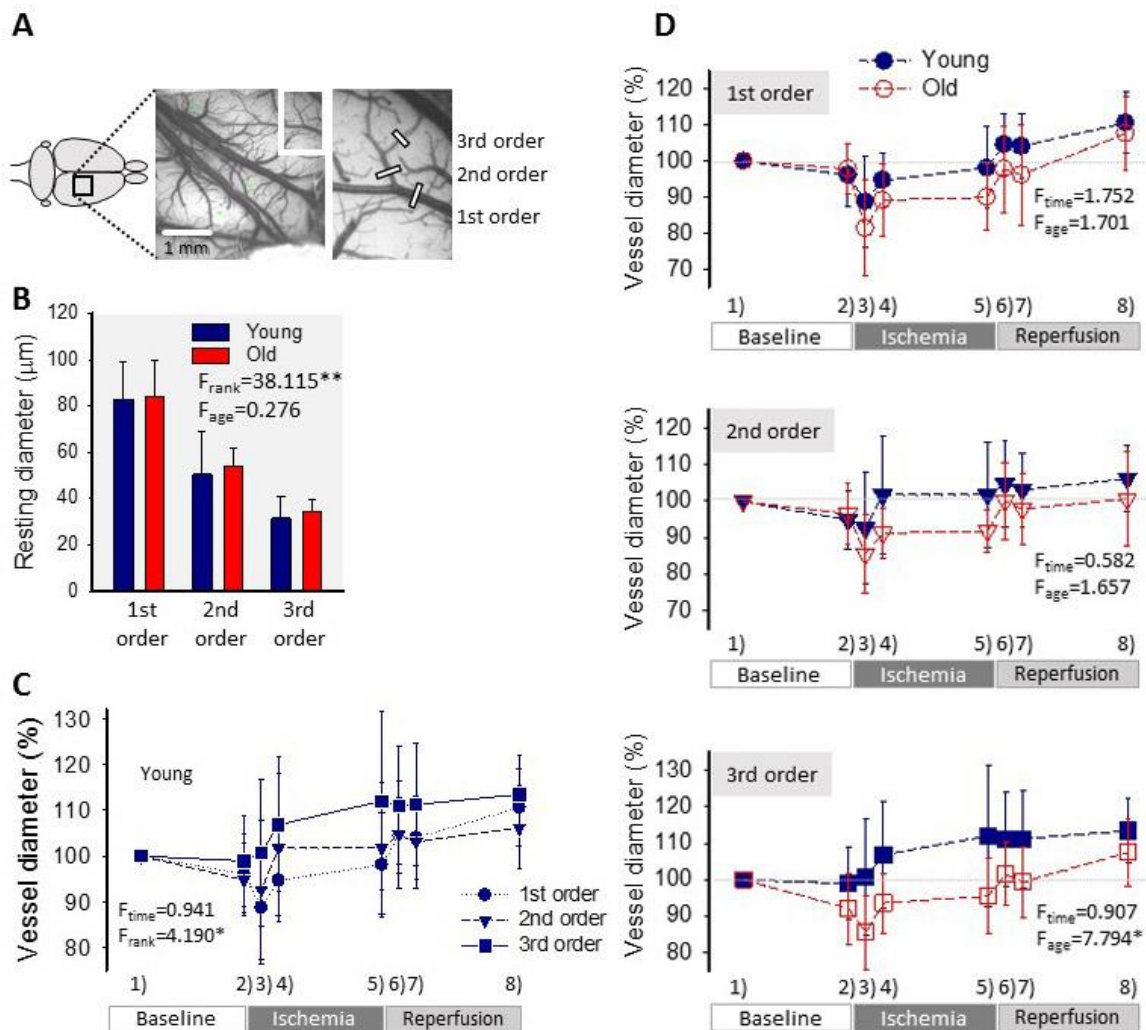
Figure 6. Pial arteriolar diameter between subsequent events of the experimental protocol. **A,** A green intrinsic optical signal (IOS) image of a representative young preparation demonstrates the ranking of pial arterioles. **B,** Resting diameter of 1st, 2nd and 3rd order pial arterioles in the two age groups. **C,** Changes of pial arteriolar diameter of 1st, 2nd and 3rd order arterioles relative to baseline (100 %) over the experimental protocol. Sampling times are: 1) baseline - prior to the elicitation of the first spreading depolarization (SD); 2) baseline - prior to ischemia induction; 3) ischemia - minimum vascular diameter after ischemia onset; 4) ischemia - prior to the elicitation of the first SD under ischemia; 5) ischemia - prior to the initiation of reperfusion; 6) reperfusion - maximum vascular diameter after reperfusion initiation; 7) reperfusion - prior to the elicitation of the first SD under reperfusion; 8) reperfusion - prior to the termination of the experiment. **D,** The impact of age on the relative changes of pial arteriolar diameter of 1st, 2nd and 3rd order arterioles. Data are given as mean±stdev (n=8/5, young/old). In **B,** a multivariate ANOVA paradigm was used for statistical analysis, considering vessel rank or age as factors (**p<0.01). In **C-D,** a repeated measures paradigm was used for statistical analysis, considering vessel rank or age as factors (*p<0.05 and **p<0.01).

The induction of ischemia in the young group was followed by a prompt diameter reduction in 1st and 2nd order arterioles (to 89±12 and 93±15 %, respectively), while the caliber of 3rd order arterioles did not change (101±16 %) *(Figure 6/C)*. The diameter of 1st and 2nd order arterioles recovered in 10 minutes to pre-ischemic values (95±8 and 102±16 %), and was maintained there until the initiation of reperfusion (98±11 and 102±14 %). At the same time, 3rd order

arterioles progressively dilated above their baseline tone over the ischemic period (107±15 and 112±19 %, 10 min after ischemia onset and shortly before reperfusion). During reperfusion, pial arteriolar diameter settled over baseline at all three levels of the pial arteriolar tree (111±8, 106±9 and 113±9 %, 1st, 2nd and 3rd order vessels). A repeated-measures ANOVA test confirmed that the calibre change of various arterioles was significantly different over the experimental protocol. *(Figure 6/C).*
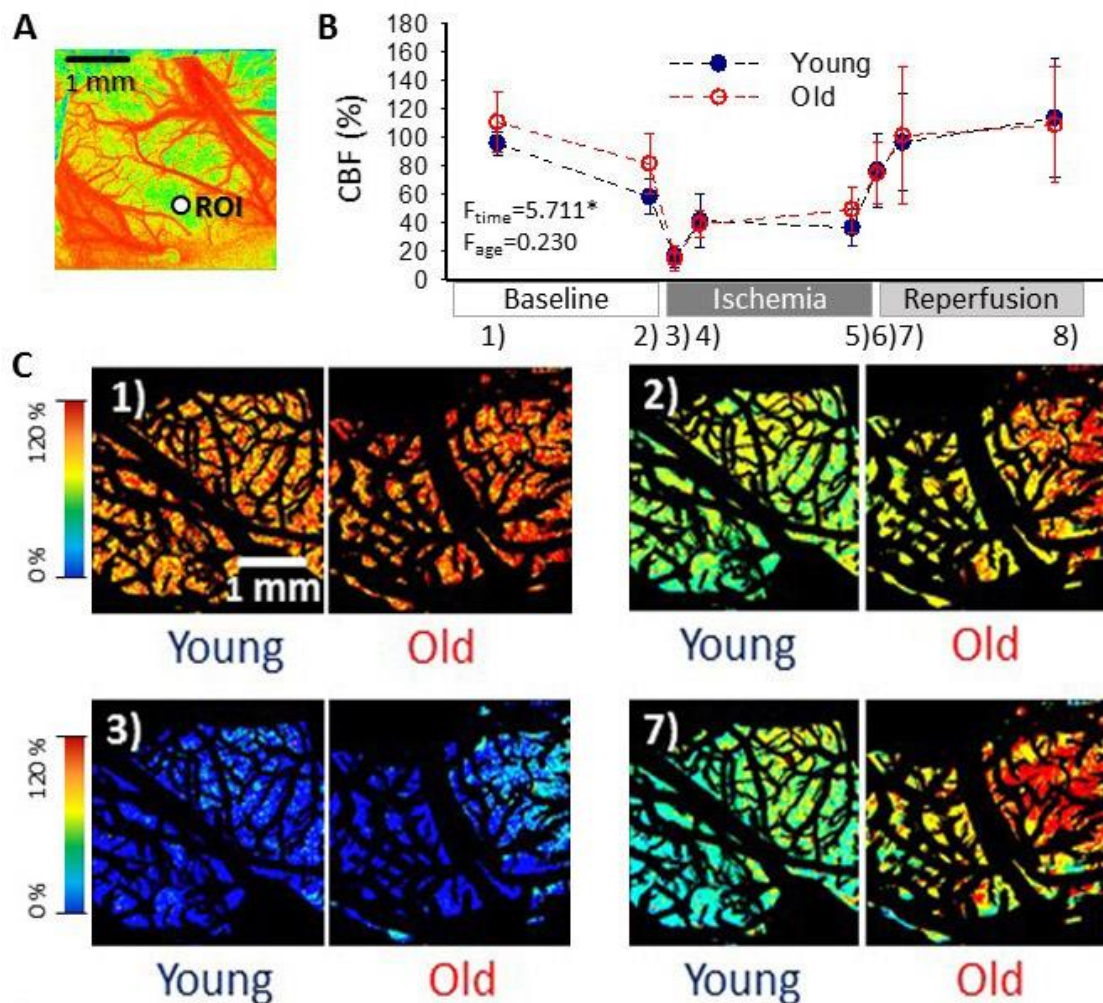

Figure 7. Cerebral blood flow (CBF) variation over the experimental protocol. **A,** A pseudo-colored, representative baseline CBF map used for single point analysis (i.e. CBF changes were extracted from a region of interest – ROI, as a function of time). **B,** Changes of local CBF relative to baseline (100 %) in the two age groups as assessed with single point analysis. Sampling times over the experimental protocol are: 1) baseline - prior to the elicitation of the first spreading depolarization (SD); 2) baseline - between SDs; 3) ischemia - minimum CBF after ischemia onset; 4) ischemia - prior to SDs; 5) ischemia – between SDs; 6) reperfusion - maximum CBF after reperfusion initiation; 7) reperfusion – between SDs; 8) reperfusion - prior to the termination of the experiment. Data are given as mean±stdev (n=9/9, young/old). Statistical analysis relied on a repeated measures paradigm with age as a factor (level of significance: *p<0.05). **C,** Computer-generated, pseudo-colored representative CBF image pairs of a young and an old preparation used for whole field analysis. The pial vasculature is masked (black) to be excluded from the analysis targeting the cortical parenchyma. The sampling time given numerically in the upper left hand corner corresponds to the numbering used in panel B.

In the old animals, diameter changes of 1st and 2nd order arterioles were similar to that observed in the young group. However, 3rd order arterioles appeared less able to dilate under ischemia *(Figure 6/C)*. In particular, in the old rats, a marked reduction in 3rd order arteriole diameter was noted upon ischemia induction (86±10 vs. 101±16 %, old vs. young), dilation over the first 10 min of ischemia reached a lower level (94±8 vs. 107±15 %, old vs. young), and remained so until reperfusion onset (96±10 vs. 112±15 %, old vs. young).

Variations of local CBF were estimated at a ROI most distant from the site of SD elicitation. As expected, the occlusion of the common carotid arteries caused a sudden drop of CBF (to 16±8 and 15±9 % of baseline, young and old), which settled at around 40 % during the period of ischemia (41±19 and 39±10 %, young and old). CBF recovered gradually during reperfusion from about 75 % measured shortly after the release of the common carotid arteries (77±26 and 75±21 %, young and old) to approximately 110 % taken prior to the termination of the experiments (114±41 and 109±41 %, young and old). No meaningful difference was observed between young and old rats *(Figure 7/B)*.

Next, flow distribution within the field of view at selected sampling times was evaluated *(Figure 7/C, Figure 8)*. The flow ranges displayed a normal distribution at rest, and a considerable portion of the field of view fell in the perfusion ranges of 91-100 % CBF (30±5 and 34±4 % of the total area, young and old) and 101-110 % CBF (24±9 and 33±9 % of the total area, young and old). After the passage of 3 SDs, the most represented perfusion range was 51-60 % CBF in the young (26±12 % of the total area), and 61-70 % CBF in the old group (19±12 % of the total area), corresponding to the long-lasting oligemia that ensues SD. The flow distribution was clearly skewed to low perfusion ranges shortly after ischemia onset. In both age groups, most of the field of view was severely hypoperfused, falling in the CBF ranges of 1-10 % (48±29 and 47±27 % of the total area, young and old) and 11-20 % (34±13 and 38±18 % of the total area, young and old). Perfusion recovered to some extent between SD events, when the most represented perfusion range appeared to be 21-30 % CBF (31±19 and 25±14 % of the total area, young and old). Finally, reperfusion resulted in the widest flow distribution, and the most remarkable difference in the spatial pattern of CBF between the young and old groups. In the young animals, nearly half of the field of view was occupied by perfusion ranges between 31-70 % CBF, the 41-50 % CBF range being just about the most represented (13±11 % of the total area). In contrast, in the old rats, approximately half of the visible cortex was

involved in the perfusion ranges of 71-110 % CBF, and the 91-110 % CBF range engaged the largest area (13±6 % of the total area).
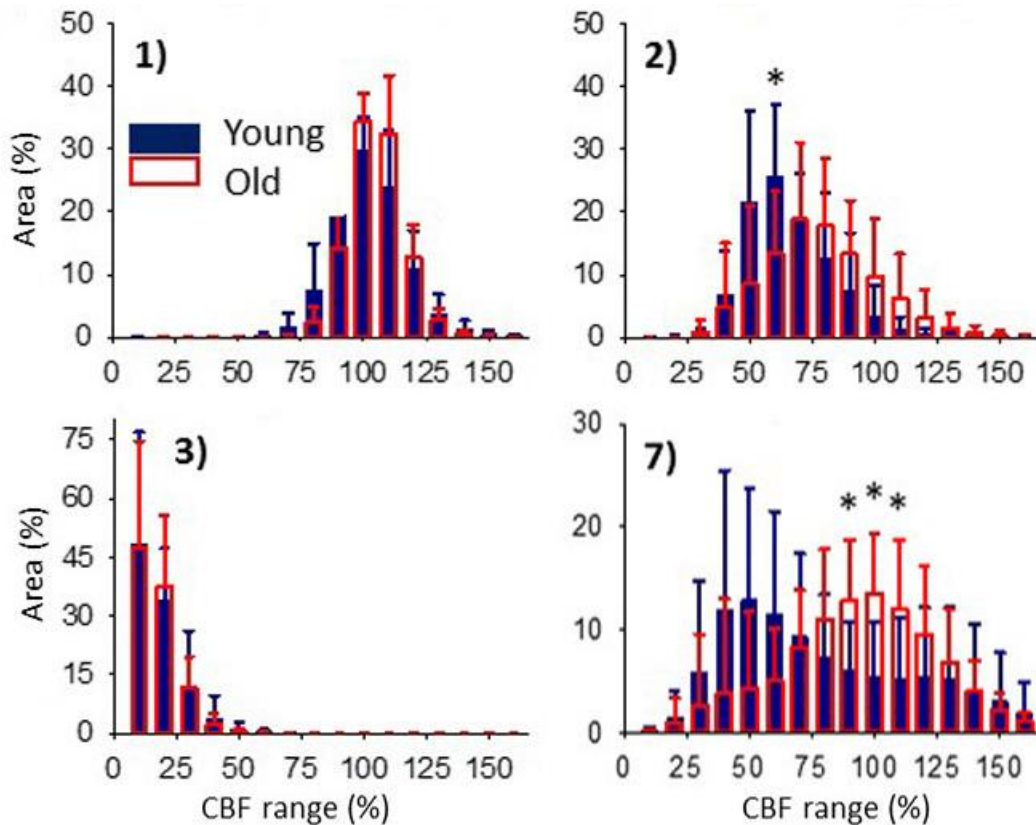

Figure 8. Cerebral blood flow (CBF) variation over the experimental protocol. Spatial flow distribution of the CBF maps, demonstrated as the relative area occupied by given CBF ranges (shown at an increment of 10 %). Data are given as mean±stdev (n=9/9, young/old). A one-way ANOVA was used to test age-related differences (*p<0.05). The sampling time given numerically in the upper left hand corner corresponds to the numbering used in Figure 7 panel B.

3.1.3. Changes of pial arteriolar diameter and CBF: Response to SD

The representative traces in *Figure 9* demonstrate that pial arterioles readily responded to SD events in the normally perfused cortex, but SD-related vascular reactivity remained obscure during ischemia. During the reperfusion phase, as a rule, vasodilation with SD was as obscure as under ischemia, but was observed occasionally (in 2 young and 1 old rats). The CBF response to SDs was dominated by considerable hyperemia, which clearly stood out during the ischemia and reperfusion phases of the experiments – at the absence of reliably detectable, concomitant pial arteriolar dilation. Because diameter changes of pial arterioles were reproducible in

response to baseline SDs only, the detailed analysis focused on this first phase of the experiments.

The first SD was coupled with obvious, transient vasodilation (to 124±15, 125±26 and 122±18 %, 1st, 2nd and 3rd order arterioles in young) and subsequent vasoconstriction (to 93±6, 94±5 and 95±3 %, 1st, 2nd and 3rd order arterioles in young) corresponding to considerable transient hyperemia (209±30 % CBF in young) and successive oligemia (65±22 % in young, *Figure 9/C*). Likewise, recurrent SD events (elicited at a time when oligemia caused by the first SD was still persistent) were associated with an increase of pial arteriolar diameter (to 123±11, 125±23 and 129±27 %, 1st, 2nd and 3rd order arterioles in young) and marked hyperemia (198±44 % CBF in young).
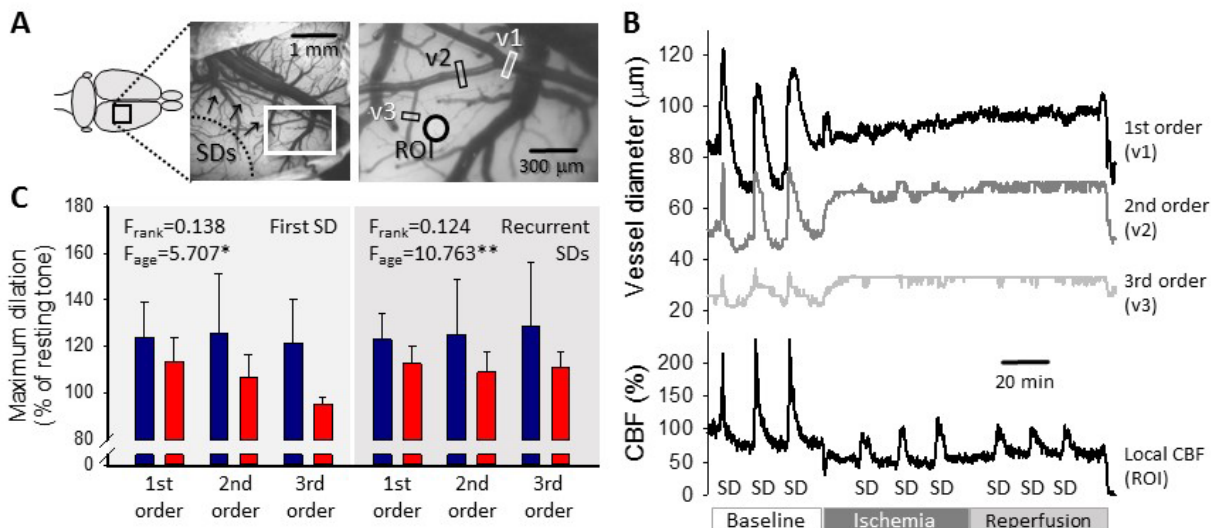

Figure 9. Representative traces of the variation in pial arteriolar diameter and local cerebral blood flow (CBF) with spreading depolarization (SD) events in a young preparation, and maximum dilation of pial arterioles in response to SDs elicited during baseline. **A,** A representative field of view over the parietal cortex of a young rat at green light illumination. Pial arteriolar segments used for the measurement of diameter changes in Panel B are indicated (v1: 1st order, v2: 2nd order, v3: 3rd order arteriole). A region of interest (ROI) designates the origin of the local CBF trace in Panel B. **B,** The dilation of pial arterioles in response to SD events (top), with the corresponding changes in local CBF (bottom) in a representative young preparation. **C,** Maximum dilation of 1st, 2nd and 3rd order pial arterioles in response to the first and recurrent SDs in normally perfused cortex in the two age groups. Data are given as mean±stdev (SD1: n=7/6, young/old; recurrent SD: n=13/13, young/old). A multivariate ANOVA paradigm was used for statistical analysis, considering vessel rank or age as factors (*p<0.05 and **p<0.01).

Age exerted a significant impact on cerebrovascular reactivity to SD. Pial arteriolar dilation proved to be less remarkable with the first SD (1st, 2nd and 3rd order arterioles: 114±10 vs. 124±15, 107±9 vs. 125±26 and 109±9 vs. 122±18 %, old vs. young,) and recurrent SDs (1st, 2nd and 3rd order arterioles: 113±7 vs. 123±11, 109±9 vs. 125±23 and 111±6 vs. 129±27 %, old vs. young). Accordingly, in the old animals, the peak of hyperemia in response to SD fell

behind (first SD: 174±33 vs. 203±33 %, old vs. young; recurrent SDs: 182±57 vs. 198±44 %, old vs. young), as reported earlier[20].

For the characterization of spatial flow distribution in the cortex when SD-associated hyperemia ruled the field of view *(Figure 10/A)*, histograms *(Figure 10/C)* in addition to the area representation of perfusion ranges *(Figure 10/B)* were evaluated. While the analysis of perfusion ranges offered only trends (e.g. the most represented perfusion ranges for recurrent SDs were 141-160 % in young and 121-140 % in the old) *(Figure 10/B)*, the histograms provided more refined information. As such, the peak of the histogram fell at a significantly lower CBF value in the old than in the young group (137±35 vs. 167±28 %, old vs. young) *(Figure 10/C, D)*, indicating a shift to the lower perfusion ranges on the CBF axis.
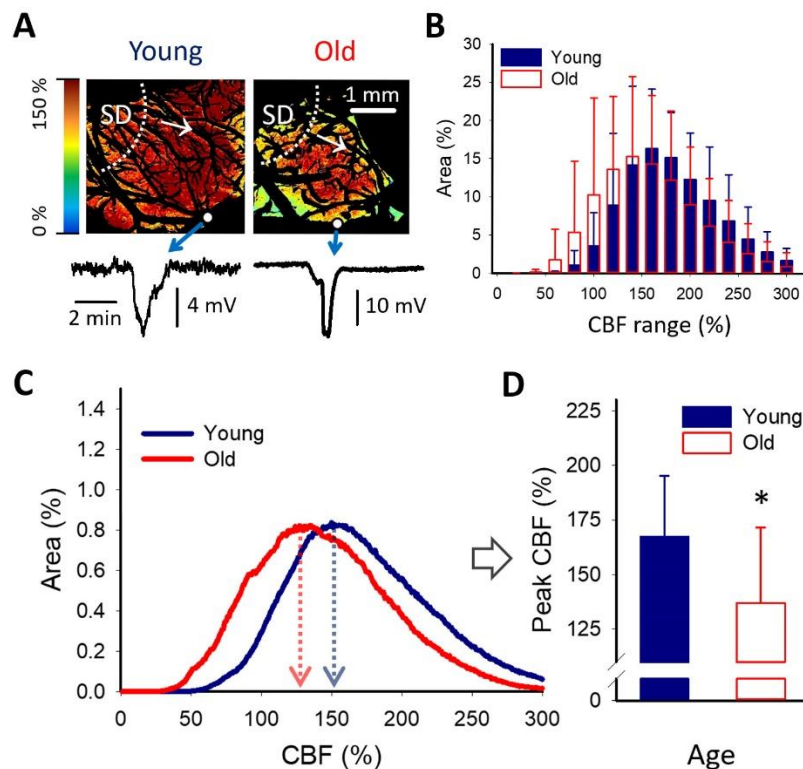

Figure 10. The spatial distribution of cerebral blood flow (CBF) at peak hyperemia in response to spreading depolarization (SD) elicited in normally perfused cortex. **A,** Representative CBF maps of a young and an old animal demonstrate flow distribution with the passage of peak hyperemia in response to recurrent SD. The SD event was confirmed by the transient negative shift of the DC potential (bottom). Small white spheres in the images show the position of the microelectrodes implanted to the cortex. White dotted lines and arrows indicate the origin and radial direction of propagation of SD. **B,** Relative area occupied by given CBF ranges (shown at an increment of 10 %) under the passage of peak hyperemia with recurrent SDs triggered in normally perfused cortex. Data are given as mean±stdev. A MANOVA paradigm was used to test age-related differences. **C,** Histograms (mean for each age group) to demonstrate the relationship between CBF and surface area of the cerebral cortex with recurrent SD. **D,** CBF at the peak of the histograms shown in Panel C. Data are given as mean±stdev (n=10/10, young/old). An independent samples T-test was used to statistically evaluate age-related differences (*p<0.05).

3.2. Series 2

The amplitude of the negative DC potential shift corresponding to SDs fell on a continuum, as shown in *Figure 11*, ranging between 0.99 and 19.44 mV. SDs with various DC potential shift amplitude were evenly distributed between age groups and phases of the experiments, establishing no particular impact of age or ischemia (two-way ANOVA: $F_{age} = 0.460$, $F_{phase} = 0.773$).
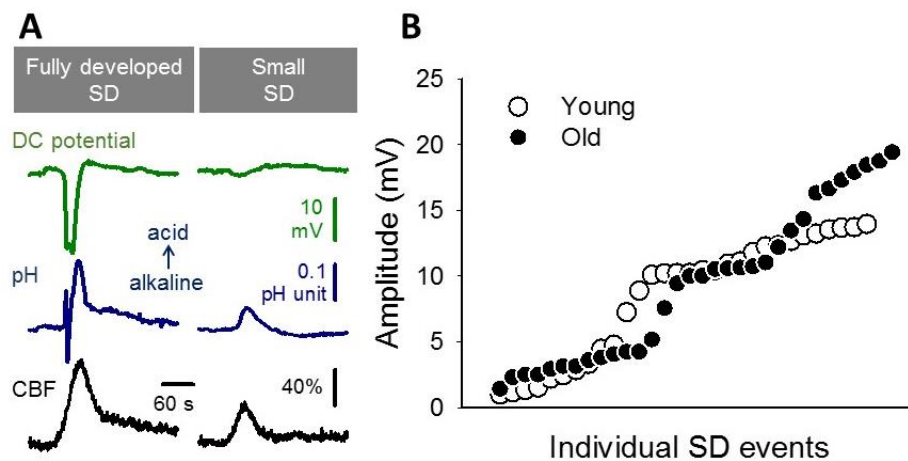

Figure 11. Variations in the amplitude of the negative direct current (DC) potential shift indicative of spreading depolarization (SD). **A,** Representative traces of tissue pH and cerebral blood flow (CBF) changes demonstrate signals corresponding to a conventional, fully developed DC signature of an SD (i.e. amplitude of the negative DC shift greater than 5 mV) (left), and a small SD (i.e. amplitude of the negative DC shift smaller than 5 mV) (right). **B,** Distribution of SD-related DC shift amplitudes. Each symbol represents a single SD event. All three phases of the experiments (i.e. baseline, ischemia and reperfusion) are included.

For the evaluation of the metabolic consequences of SDs, the association between the amplitude and duration of the DC potential shift, related acidosis, and hyperemia was analyzed in detail. During baseline, in young animals, the amplitude of all three variables was tightly coupled (e.g., DC potential shift and hyperemia: $r = 0.819$, *p < 0.05; *Figure 12/B, C*), whereas their duration appeared to be unrelated to each other (e.g., DC potential shift and hyperemia: $r = 0.176$; *Figure 12/E, F*).

Under ischemia, the amplitude of hyperemia dissociated from the amplitude of both the DC potential shift and acidosis ($r = 0.236$ and $r = 0.429$, respectively) and remained uncoupled during reperfusion as well *(Figure 12/B, C)*. At the same time, the positive correlation between the amplitude of the DC potential shift and acidosis continued to be unaffected by ischemia ($r = 0.789$, *p < 0.01; *Figure 12/B*). The durations of the three variables independent under

baseline became interrelated over the ischemic phase (e.g., DC potential shift and acidosis: $r = 0.935$, **p < 0.01$) and lost correlation again during reperfusion *(Figure 12/E, F)*.
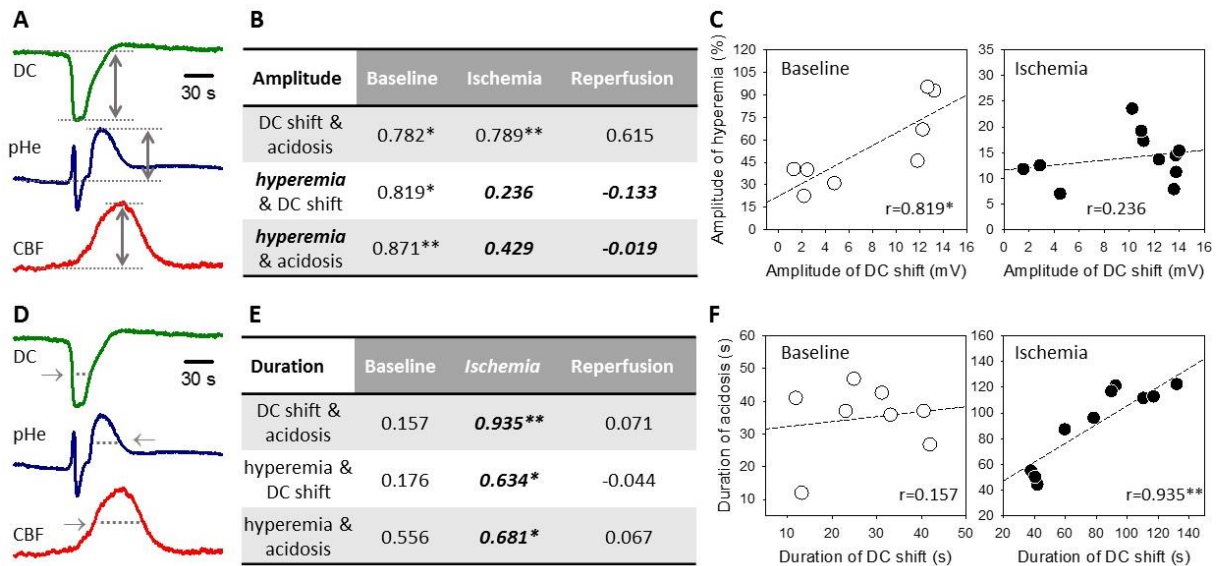

Figure 12. Correlation analysis considering the amplitude (A-C) and duration (D-F) of the spreading depolarization (SD)-related direct current (DC) potential shift, transient tissue acidosis and hyperemic response, to reveal the impact of aging. **A & D**, Illustration of the variables considered for the analysis. **B,** Overview of correlation coefficients delivered by a Pearson two-tailed paradigm (*p<0.05, **p<0.01) for the association of amplitudes in the young group, for each of the three subsequent phases of the experiments. Alteration of correlation coefficients is highlighted in bold italic font. **C,** Representative plots demonstrate the impact of ischemia on the correlation between the amplitude of the DC potential shift indicative of SD and that of the related hyperemia. **E,** Overview of correlation coefficients delivered by a Pearson two-tailed paradigm (*p<0.05, **p<0.01) for the association of durations in the young group, for each of the three subsequent phases of the experiments. Alteration of correlation coefficients is highlighted in bold italic font. **F,** Representative plots to demonstrate the impact of ischemia on the correlation between the duration of the DC potential shift indicative of SD and that of the related tissue acidosis. Open symbols stand for baseline; black symbols represent ischemia.

Aging exerted a discernible effect on the amplitude of the three variables during baseline *(Figure 13)*. Strikingly similar to the impact of ischemia, old age uncoupled the amplitude of hyperemia from that of the DC potential shift and acidosis ($r = 0.221$ and $r = 0.249$, respectively), whereas it left the amplitude of the DC potential shift and acidosis strongly correlating ($r = 0.998$, **p < 0.01$) comparable to young age *(Figure 13/B, C)*.

Finally, aging dissociated the duration of acidosis from the duration of the DC potential shift and hyperemia under ischemia ($r = 0.482$ and $r = 0.286$, respectively), whereas it did not alter the baseline association between the length of the DC potential shift and hyperemia ($r = 0.657$, *p < 0.05$; *Figure 14/B*). The age-related uncoupling of acidosis from the other variables was clearly due to the marked elongation of the duration of acidosis relative to the other variables in the old group *(Figure 14/C)*. More specifically, the length of acidosis was ~40% longer than the DC potential shift in young animals while almost doubled relative to the duration of the DC

potential shift in old animals. Remarkably, the duration of acidosis was relatively shorter than the duration of hyperemia in young animals but exceeded the duration of hyperemia in old animals *(Figure 14/C)*. Finally, it is noteworthy that the relative duration of hyperemia was gradually decreasing (195% to 172% to 167%, young baseline to young ischemia to old ischemia, respectively), whereas the relative duration of acidosis was increasing with ischemia and age (127% to 140% to 192%, young baseline to young ischemia to old ischemia, respectively; *Figure 14/C*).

Figure 13. Correlation analysis considering the amplitude of the spreading depolarization (SD)-related direct current (DC) potential shift, transient tissue acidosis and hyperemic response, to identify the impact of aging. **A,** Illustration of the variables considered for the analysis. **B,** Overview of correlation coefficients delivered by a Pearson two-tailed paradigm (*p<0.05, **p<0.01) for the association of amplitudes over baseline, for each age group. Alteration of correlation coefficients is highlighted in bold italic font. **C,** Representative plots demonstrate the impact of age on the correlation between the amplitude of the DC potential shift indicative of SD and that of the related hyperemia.

When SD events evoked during baseline were sorted on the basis of DC potential shift amplitude (i.e., <5 mV and >5 mV; *Figure 11/A*), tissue pH proved to be significantly more acidic before SDs with small DC potential shift amplitude (pH 7.20 ± 0.04 vs. 7.31 ± 0.03; *Figure 15/B*). In further support, a strong positive correlation was established between tissue pH before SD and the DC potential shift amplitude with SD ($r = 0.909$, **$p < 0.01$), which was

abolished by ischemia ($r = 0.244$) and reestablished during reperfusion ($r = 0.739$, *p < 0.05; *Figure 15/C, D*).

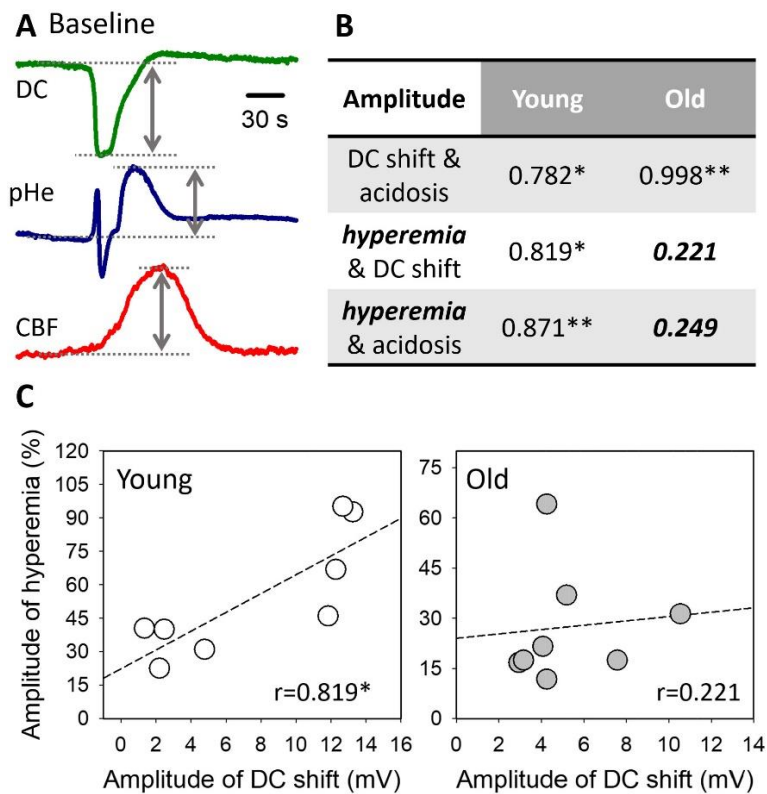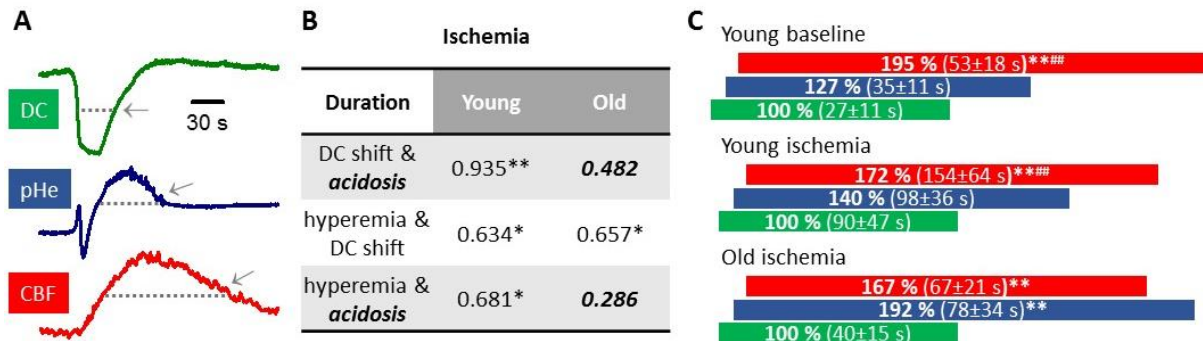**Figure 14.** Correlation analysis and relative changes considering the duration of the spreading depolarization (SD)-related direct current (DC) potential shift, transient tissue acidosis and hyperemic response, to identify the impact of aging. **A,** Illustration of the variables considered for the analysis. **B,** Overview of correlation coefficients delivered by a Pearson two-tailed paradigm (*p<0.05, **p<0.01) for the association of durations over ischemia, for each age group. **C,** Duration of SD-related acidosis and hyperemia relative to the duration of the DC potential shift (taken as 100 %) during ischemia. Horizontal bars are color-coded according to Panel A (i.e. green: DC potential shift, blue: acidosis, red: hyperemia). Relative values (bold) were derived from the mean absolute values given in brackets (mean±stdev). A one-way analysis of variance (ANOVA) followed by a Fisher post hoc test was used for statistical analysis (Young ischemia, **F=10.962; Old ischemia, **F=13.144). Levels of significance are given as **p<0.01, vs. DC potential; ##p<0.01, vs. acidosis.

4. Discussion

The high incidence of CeVDs and their social and economic consequences are targets of intensive research. Continuous monitoring, statistical analysis in the population and animal research help to establish new prevention and rehabilitation methodologies. Following a stroke event there is an inevitable decay in its focus, but the survival of the surrounding, penumbra area is not predetermined. The understanding of these mechanisms is crucial for the developing of new effective rehabilitation methods[1–4]. In our study we have focused on the SD-related changes of pial vascular diameter, spatial dynamic of CBF response, tissue pH alterations and their correlations.

4.1. Series 1

Our data reveal that the dilation of pial arterioles, which is a prompt reaction to SD[9,11,62,63] is less efficacious in the aged compared to the young rat cerebral cortex, down to the smallest arterioles the resolution of our approach allowed to investigate (a diameter of ~30–35 μm at rest). Our results are consistent with previous reports showing that the endothelium-dependent dilation of pial arterioles in response to the topical application of vasodilator agents

(acetylcholine or bradykinin) or systemic hypercapnia is considerably smaller in aging than in young adult rodents[31,64]. Despite the similar age-related reduction of endothelium-dependent and SD-linked vasodilation, the cellular signaling may not necessarily be identical, since the role the endothelium may play in regulating the CBF response to SD is still uncertain[11]. The likely cause of the age-related reduction of endothelium-linked vasodilator ability is thought to be oxidative stress[29]. SD itself has been shown to induce oxidative stress as evidenced by the increased level of the lipid peroxidation product malondialdehyde in association with SD[65], but it has not been explored how oxidative stress might modulate the CBF response to SD, and how age might interfere with the signaling.
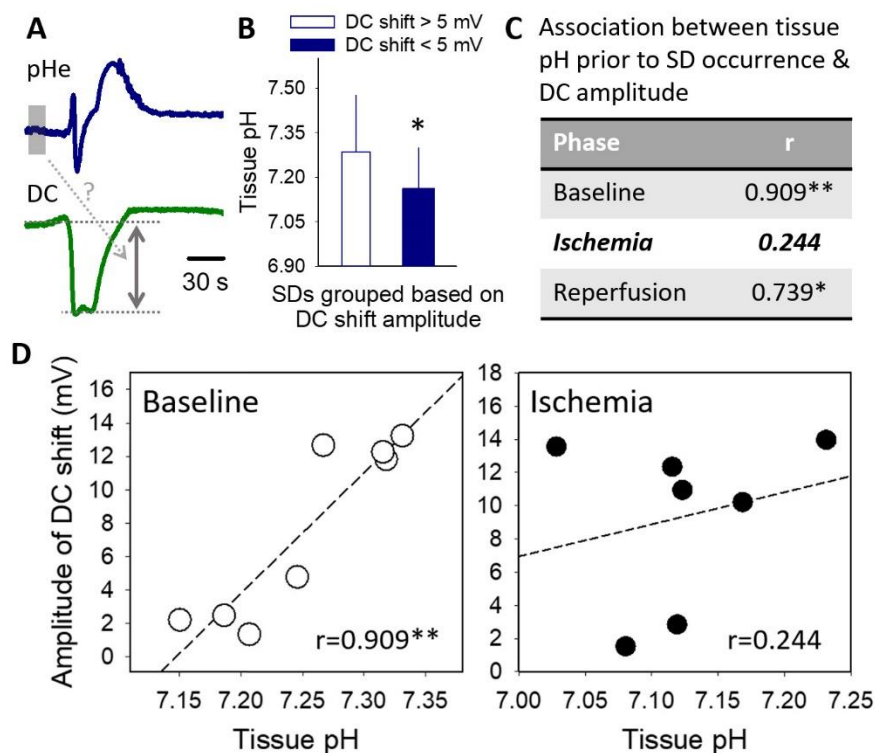
Figure 15. Association between tissue pH prior to spreading depolarization (SD) and the amplitude of the direct current (DC) potential shift with SD. **A,** Illustration of the origin of data sets analyzed. **B,** Tissue pH prior to SD events evoked during baseline, events sorted based on DC shift amplitude. **C,** Correlation coefficients delivered by a Pearson two-tailed paradigm (*$p<0.05$, **$p<0.01$) for the association of variables in the young group, for each of the three subsequent phases of the experiments. The impact of ischemia on the correlation coefficient is highlighted in bold italic font. **D,** Graphic illustration of the impact of ischemia on the correlation between tissue pH and the amplitude of the SD-related DC shift. Open symbols stand for baseline; black symbols represent ischemia.

The observation concerning the pial arterioles in the present study was found relevant for the intact cortex alone because SD-related pial vasodilation remained undetectable during ischemia and reperfusion. This was not anticipated because hyperemic CBF responses were recorded repeatedly under ischemia earlier[16,20,54] and here with the very same SDs (*Figure 9*).

One might postulate that the SD-related dilation of pial vessels remained undetectable because the vessels had already reached their maximum diameter in compensation for ischemia onset or as their reaction to reperfusion. This may be an attractive explanation, but vasodilation during ischemia or reperfusion did not exceed a diameter increase of 110–115% relative to resting tone in the current experiments, while the maximum SD-coupled dilation of the same arterioles in the intact cortex (i.e., recorded over the first, baseline phase) proved to be 120–130%. These data imply that the full dilation capacity of pial arterioles was not exhausted during ischemia/reperfusion to account for the consequential lack of vasodilation with SD on ischemic background—instead, ischemia is suggested to have caused a potential impairment of arteriolar reactivity.

The dissociation of pial arteriolar diameter and local CBF variations may not be unusual. The caliber changes of pial arterioles may not strictly comply with local parenchymal CBF variations associated with SD[11]. Indeed, the SD-coupled CBF elevation appears to correlate better with the tone adjustment of finer arteriolar branches located deeper in the cortex[11,66]. The dilation of pial arterioles in response to neuronal activation has been suggested to evolve as the result of a retrograde, upstream propagation of vasodilator signals[67]. This process is thought to cause a conducted hyperpolarization of cerebrovascular smooth muscle cells or to be the result of transendothelial signaling, which originates in parenchymal microvessels[68,69]. If this scheme is valid—at least in part—in the context of SD-associated vasodilation, the local hyperemia detected with LASCA in the ischemic cortex here could reflect an initial, microvascular dilation. Yet, upstream vascular conductance may have failed, and, as a result, vasodilation did not manifest at the level of the pial arterioles. Alternatively, it is also plausible that the dilation of pial arterioles with SD is caused by vasoactive substances released directly at the vessels—rather than being conducted from deeper cortical layers. Unlike parenchymal arterioles, pial arterioles are innervated by perivascular nerves originating from various ganglia (e.g., trigeminal, superior cervical), are not encapsulated by astrocytic endfeet, and are constantly bathed in cerebrospinal fluid[11]. Due to their distinct anatomical position among cerebral vessels,

pial arterioles may be selectively desensitized to vasoactive signals during ischemia, or their specific innervation may become preferentially impaired.

Because pial vasoreactivity to SD is undetectable during ischemia/reperfusion in either of the two age groups, investigating the impact of age on this variable under ischemia/reperfusion has become redundant. However, our previous data have shown that the magnitude of SD-associated hyperemia decreased with age under ischemia/reperfusion[17,20]. Here, we demonstrate that the density of the pial vasculature was not altered in our aging rats (*Figure 5*). These observations suggest that age-related functional impairment rather than structural maladaptation may be the underlying pathology causing the detected failure of the hyperemic response to SD. We have made a number of additional observations with regard to aging.

First, the resting diameter of pial arterioles of the parietal cortex proved to be similar in young and aged rats (*Figure 6/B*), indicating an intact maintenance of resting cerebral arteriolar myogenic tone.

Second, ischemia induction provoked compensatory vasodilation particularly in small-caliber pial arterioles in young rats, a reaction which appeared to be impaired in old animals (*Figure 6/C,D*). The occlusion of the common carotid arteries was promptly followed by a transient drop of arteriolar diameter (probably due to the sudden fall of perfusion pressure and the transient cessation of blood flow in branches of the middle cerebral artery), before pial vasodilation occurred. The caliber regulation of the pial arterioles following ischemia onset is subject to reduced perfusion pressure, which initiates myogenic—and metabolic—responses to adjust arteriolar tone. The drop in perfusion pressure must be compensated by decreasing vascular resistance (i.e., vasodilation) in order to maintain optimal blood flow. This compensatory vasodilation (thought to be an intrinsic reaction of cerebrovascular smooth muscle cells) clearly evolved in the pial arterioles of our young rats but was less obvious in old animals (*Figure 6*). Production of the vasodilator nitric oxide may be an additional response to the slow re-establishment of blood flow (i.e., increasing shear stress) due to the flow re-distribution at the level of the circle of Willis after carotid occlusion. Nitric oxide production has been linked, for example, to the augmentation of collateral flow in experimental models of focal cerebral ischemia[70]. Taken together, the results suggest that cerebral arterioles in the aging brain are less able to respond to a pressure drop or metabolic challenge optimally, in line with the insufficiency of the CBF response to SD[20] neuronal activation[28,30], or hypercapnia[31].

The endothelium is likely implicated in the arteriolar response to ischemia induction. Endothelial dysfunction in the context of cerebrovascular aging has been extensively studied[39]. Oxidative stress has been recognized as a central molecular mechanism damaging endothelial function[71]. Importantly, the superoxide anion is generated in the cerebral vasculature by activation of NAD(P)H oxidase, which is augmented by aging[29]. The increased levels of superoxide anion in the aged brain quickly reacts with nitric oxide to produce peroxynitrite, and to impair endothelial nitric oxide synthase-based reactivity of cerebral arterioles. This sequence of events may have contributed to the less efficient vasoreactivity upon ischemia induction in our old rats.

Third, CBF between SD events did not differ between age groups (*Figure 7/B*). Of note, SD is followed by a long-lasting oligemia (duration >30 min), which in our experimental paradigm did not resolve prior to the elicitation of recurrent SDs (i.e., inter-SD interval was 15 min). Post-SD oligemia is apparently mediated by 20-HETE production in vascular smooth muscle cells[72] or the synthesis and release of vasoconstrictive prostanoids[73]. On the basis of our observations, this vasoconstrictive signaling appears to be essentially preserved during the aging process.

Finally, the analysis of spatial CBF distribution revealed that a greater proportion of the aged cortex—compared to the young—was involved in higher perfusion ranges during reperfusion (*Figure 7/C, Figure 8*). It has been proposed that CBF may exceed the resting level during reperfusion because ischemia-generated oxidative/nitrosative stress disrupts the actin cytoskeleton in cerebrovascular smooth muscle cells, which leads to diminishing myogenic tone and reduced cerebrovascular resistance[74,75]. The re-establishment of blood supply to the forebrain thus allows blood flow into a dilated cerebrovascular network, which causes hyperperfusion. This sequence of events suggests that, in our experiments, the ischemic-stress related dilation of the cortical microvasculature was more extensive in the old rats, possibly because of more accentuated oxidative/nitrosative stress typical of the old compared to the young nervous tissue. In turn, the hyperperfusion is thought to contribute to reperfusion injury by initiating a neuroinflammatory response and a further overproduction of reactive oxygen species[76], thereby possibly operating a vicious cycle. Our finding raises the possibility that this pathophysiological cascade of events may become more prevalent in the aged brain.

Accumulating evidence identifies SD as a biomarker and a potent pathophysiological contributor to ischemic lesion expansion[46,77], possibly because of the insufficiency of the flow

response or the vascular steal effect it provokes[12,13,57,78] and the poor recovery from the SD-induced acidic pH shift. Age has been identified to accelerate infarct maturation after ischemic stroke[40–42]. Here we provide supportive evidence, that in addition to insufficient hyperemia, the SD coupled pial vasodilation - if detectable - is compromised by old age. This impaired vasoreactivity, in turn, may contribute to a worse outcome of ischemic brain injury. Our study supports the concept that the functional impairment - rather than vascular rarefaction - may be a leading cause of the age-related deficit of the CBF response to SD, and possibly with neurovascular coupling at large. Structural abnormalities of the cerebral vasculature are also expected to exert an additional impact on flow dynamics when present. Finally, we formulate the concept that reperfusion injury may be graver in the aging compared to the young brain, because CBF during reperfusion tends to fluctuate in higher perfusion ranges, with the potential of predisposing the tissue for increased oxidative stress and inflammation.

4.2. Series 2

The recording of DC potential is a conventional, robust experimental technique, which has been routinely used for over seven decades to identify SD occurrence in the cerebral cortex of anesthetized animals, in *in vitro* brain slice preparations, and, most recently, in brain injury patients[10,79,80]. The DC potential shift representing the sum of neuronal and glial depolarization reflects gross ionic translocations between the intra- and extracellular compartments and correlates well with the extracellular surge of K^+ with SD[10,81,82]. Recurrent SDs in the injured brain of patients are perceived to mark and to exacerbate metabolic failure and excitotoxic injury[12,46,77], especially because the long cumulative duration of recurrent SDs has emerged as an early indicator of delayed ischemic brain damage[49,77]. Still, it has remained largely unexplored whether the SD-related metabolic challenge could possibly be estimated by examining and evaluating the quantitative characteristics of the negative DC potential shift of individual SD events. Additionally, the novel imaging methods (intrinsic optical signal, LASCA, fluorescent ion or pH sensitve dyes) help to examine the above events in a broader spatial range and give extensive information about the neighbouring areas too. Proving direct coupling between depolarization, CBF response, vascular reactivity and the tissue pH variations with SD should foster the understanding of the pathophysiological sequence and significance of events initiated by SD in the injured brain.

The recording of the DC potential is an inherent component of the assessment of tissue pH variations with the use of ion-sensitive microelectrodes[60], which, therefore, allows the direct comparison of the two synchronous signals. Still, thorough correlation analysis between quantitative features of the DC potential shift and acidosis with SD has not been presented. Investigators exploring tissue pH changes with SD relying on microelectrodes focused on the cellular mechanisms of pH regulation[83] or examined the close relation between the elevation of lactate and the decrease of tissue pH[84]. Later in vitro studies have concentrated on the short-lasting alkalotic shift that precedes the SD-related acidosis with the purpose to dissect its role in the potential facilitation of SD occurrence in the ischemic nervous tissue and left the subsequent phase of longer-lasting acidosis unattended[85,86].

Here, we present that the amplitude of the SD-related DC potential shift and that of acidosis strongly correlate in the intact rodent cortex, and this association persists steadily under ischemia and in the aged brain. These findings suggest that the positive coupling between the amplitude of the DC potential shift and subsequent acidosis with SD is highly conserved, and a larger shift of the DC potential predicts a more pronounced acidic peak with SD. Assuming that a greater shift in the DC potential indicates more intensive depolarization and accepting that neuronal activity is directly followed by an increase in intra- and extracellular acid load, as shown in experimental models, as well as by noninvasive imaging of the human brain[87,88], it is reasonable to anticipate that a larger DC potential shift, as shown here, yields deeper acidosis. Our correlation analysis here demonstrates that the peak of hyperemia in response to SD is directly proportional to the amplitude of the DC potential shift and that of acidosis in the intact cortex. This result is consistent with the outcome of fundamental positron emission tomography studies, which concluded that local CBF was linearly coupled with neuronal activity in response to visual stimulation under physiological conditions[89]. Furthermore, a recent report[33] has also confirmed this association by showing larger whisker stimulation-evoked CBF responses, together with the intensification of neuronal activity in the intact rodent cortex. Finally, it appears that tissue pH decreasing transiently with SD can modulate the amplitude of the ensuing CBF response (*Figure 16*). The perceived causality would support the idea that local CBF regulation with SD must have an effective metabolic component[45], in addition to the more accepted neurovascular coupling hypothesis[11].
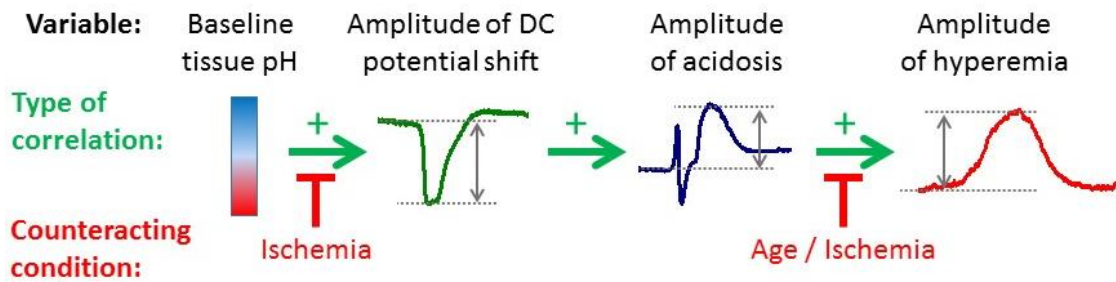
Figure 16. Conceptual overview of the causal sequence of associations between the amplitudes of variables, as proposed on the basis of the current analyses.

We have found that the correlation between the amplitude of hyperemia and that of the DC potential shift or acidosis with SD becomes lost under ischemia. Ischemia is known to impair neurovascular coupling, as demonstrated by the attenuation of functional hyperemia to forepaw stimulation in rodent models[19]. Likewise, ischemia significantly reduced the amplitude of hyperemia in response to SD, which has been systematically evaluated against SD-related hyperemia recorded in the intact cortex[16,20,90,91]. At the same time, the amplitude of the SD-related DC potential shift was shown to be resistant to ischemia[16]. These data, fortified by the present analyses, demonstrate that, even though SDs are as intense under ischemia as in the intact cortex, the CBF response becomes impaired, clearly confirming dysfunctional coupling between the two variables. In addition, we show here that not only ischemia but also healthy aging dissociates the amplitude of hyperemia from that of the DC potential shift with SD. This phenomenon is highly consistent with the well-studied adverse effect of aging on the efficacy of neurovascular coupling, which was linked to the generation of free radicals and oxidative stress[28,30].

Our laboratory reported previously that longer depression of the electrocorticogram or a longer DC potential shift with SD was associated with longer hyperemia and argued that the return of CBF to baseline after peak hyperemia was postponed by the continuing energy need of the tissue, as reflected by the sustained depolarization[16,90]. However, whether this association was valid for the intact as well as for the ischemic condition has not been distinguished. Here, we show that the longer duration of hyperemia to SD coincides with longer depolarization as well as with a longer-lasting acidosis in the ischemic brain only (*Figure 12/E*). One plausible reason for the lack of correspondence between the length of hyperemia and the DC potential shift in the intact cortex may be that hyperemia lasts disproportionately longer in the intact than in the

ischemic condition (*Figure 14/C*). This would be consistent with the notion that the CBF response to SD creates luxury perfusion in the cortex that receives uninterrupted blood supply[11]. A novel observation of this study suggests that aging disrupts the correspondence of acidosis duration with the duration of the DC potential shift and hyperemia with SD (*Figure 14/B*). At closer inspection, the relative length of acidosis increases excessively in the aged ischemic brain, which accounts for the loss of correlation (*Figure 14/C*). Acid load with SD was suggested to be caused by the accumulation of lactate[15,83,84], which is readily cleared into the bloodstream within minutes after SD is triggered in the intact young rodent cortex[92]. Considering these data, it is conceivable that the sustained acidosis with SD in the aged brain is caused by decelerated lactate efflux through the blood-brain barrier. The consequences of the exaggerated duration of acidosis are thought to be twofold. First, the threshold of acid-induced cell death was shown to be reduced with the prolongation of acid exposure[93], which may put the aging brain at a higher risk for acid-induced ischemic neurodegeneration[94]. Second, considering that acidosis outlasts hyperemia as seen here, the mismatch between these variables is perceived to indicate accentuated metabolic crisis instigated by SD in the aged brain.

As the DC potential shift indicative of SD was comprehensively analyzed here, a seemingly technical issue that has been dormant for some time was addressed. We and others regularly encounter atypical SD-associated, negative DC shifts in the intact and injured cortex, which are rather small in amplitude.

These events (*Figure 11/A*) give rise to uncertainty as to whether the small DC potential shift should be considered to indicate a true SD wave. Moreover, the metabolic consequences of these obscure events on the DC potential traces are of interest to assess their significance and injurious potential, but have not yet been examined.

The typical size of the SD-related negative DC potential shift as measured by an intracortical electrode relative to a distant ground is 15–30 mV[10]. The occasional, rather small amplitude (i.e., <5 mV) of a few SD-related DC potential shifts acquired via the same electrode, within the same preparation that also delivers typically large signals with other SDs, has been puzzling to investigators who rely on the DC potential signature to confirm SD occurrence. The ambiguity as to whether a DC potential shift of small amplitude should be considered to reflect the actual evolution of an SD can be resolved by formulating the restriction that a DC potential variation indicates an SD event only when its amplitude exceeds a given value. However, what

the threshold value should be is difficult to justify, particularly in view of our present data showing an uninterrupted spectrum of the DC potential shift amplitude within the same set of experiments (*Figure 11/B*).

It has been long accepted that low pH hampers the elicitation and propagation of SD, a notion that was corroborated by the delayed occurrence and slower rate of propagation of SD in brain slices exposed to an acidic medium[18,86]. The reason for SD suppression by low pH was suggested to be the inhibition of the *N*-methyl-D-aspartate receptors by extracellular protons[95] or the modulation of the conductance and gating properties of voltage-gated K^+, Na^+, and Ca^{2+} channels[96]. Here, we present data obtained in vivo that lower tissue pH coincides with the smaller amplitude of the DC potential shift with arising SDs, but this association is valid only in the normally perfused cortex and is lost under ischemia.

Taking our argument proposing that a smaller DC potential amplitude corresponds with an SD in its diminishing phase, we can postulate that SD events not only propagate slower at lower, albeit physiological pH[86] but also cover a shorter distance before coming to a halt.

In view of this suggestion, it is interesting to observe that lower pH does not predict smaller DC potential shift, and thus supposedly shorter SD route, in the ischemic cortex. It appears that other ischemia-related factors should overrule the inhibitory effect of low pH on SD propagation. It is conceivable, for instance, that glutamate, which accumulates excessively in the ischemic nervous tissue[97,98] and has been recognized to facilitate the spreading of depolarization via *N*-methyl-D-aspartate receptor and voltage-gated Ca^{2+} channel activation[81,99,100], overrides tissue acidosis and promotes SD propagation. Furthermore, extracellular K^+ has also been implicated in sustaining SD propagation[81,101], and, like glutamate, it is elevated in the ischemic tissue over physiological levels (e.g., from 2–4 mM up to 9–12 mM) that favor SD evolution[102,103]. Taken together, the inhibitory impact of tissue acidosis on SD propagation under ischemia is suggested to be negligible compared with the facilitating role of high interstitial concentration of glutamate, K^+, or their combination.

Our laboratory's recent[20] and present results together implicate tissue acidosis in the mediation of SD-related neurodegeneration, especially in the aged brain, due to the poor recovery from the SD-induced acidic pH shift. Appreciating that the apparent, persisting elevation of lactate concentration accounts for the SD-related tissue acidosis[83,84,104], hampered lactate removal is thought to be a potential pathomechanism sustaining low tissue pH in the aged brain. The

facilitated diffusion of lactate to the bloodstream is mediated by monocarboxylic acid transporter 1 (MCT1) located on endothelial cells that form the blood-brain barrier[105]. The dysfunction of MCT1 was previously perceived to contribute to acid-related neurodegeneration in ischemic stroke[106]. Furthermore, MCT1 expression was found strongly age-dependent in the juvenile brain[107,108], although no evidence can be retrieved to demonstrate how MCT1 expression or activity might be altered by old age. Taken together, it is conceivable that MCT1 downregulation or dysfunction at the aged blood-brain barrier could possibly impede lactate removal, thereby prolonging SD-induced lactate acidosis, and accelerate ischemia-related neurodegeneration. If this proposition stands true, potentiating the efficacy of MCT1 function in the aged cortex under ischemia could possibly improve injury outcome after stroke. The validity of the above hypothesis should, however, be scrutinized by upcoming research.

5. Conclusion

The incidence of acute ischemic stroke doubles every 5 years over 50 years of age, and the conversion of the ischemic penumbra tissue to the infarction is accelereated at old age, as well[40]. Overall, ischemic stroke occurs exponencially more frequently with advancing age in the elderly population, and leads to worse neurological outsome. These circumstances highly encourage investigations to explore the impact of age on the pathophysiology of ischemic stroke, to understand relevant age-related maladaptive changes in the nervous tissue or the cerebrovascular system that pose a higher risk and lead to poor outcome in elderly stroke patients. Here we have focused on the impact of age on cerebrovascular and metabolic changes associated with SD, because SD has been understood as the principal mechanism of lesion progression in acute brain injury[46]. We have found that

(i)   We have found that the density and resting tone of the pial and cortical penetrating cerebrovascular network is preserved with aging. However, the capacity of pial arterioles to dilate in reponse to SD has been found weaker in the old compared to the young rat brain, suggesting an age-related impairment of neruovascular coupling.

(ii)   Our experiments identified an age-related shift to a greater representation of higher flow ranges in the reperfused cortex, which carries the risk of more severe ischemia/reperfusion injury in the old brain, due to more obvious oxidative stress.

(iii) Finally, we have shown that aging disproportionately increases the duration of tissue acidosis with SD. This is of importance because the prolongation of acid exposure is understood to lower the threshold of acidosis induced cell death[93], which may be thus more prominent in the aging brain.

In conclusion, we have shown that the age-related impairment of the cerebrovascular system and an increased metabolic burden imposed by SD may contribute to the worsening outcome of ischemic stroke in elderly patients.

6. Online References

I.   Eurostat. Population Structure and Ageing. Available from:
https://ec.europa.eu/eurostat/statistics-
explained/index.php?title=Population_structure_and_ageing

II.   http://strokeeurope.eu

7. References

1. Wilkins, E., L., W., Wickramasinghe, K. & P, B. European Cardiovascular Disease Statistics 2017 edition. *Eur. Hear. Netw.* 8–15; 94, 118, 127, 149, 162, 174 (2017).

2. Smolina, K., Wright, F. L., Rayner, M. & Goldacre, M. J. Determinants of the decline in mortality from acute myocardial infarction in England between 2002 and 2010: Linked national database study. *BMJ* **344**, 1–9 (2012).

3. Shah, R. *et al.* Epidemiology report: Trends in sex-specific cerebrovascular disease mortality in Europe based on WHO mortality data. *Eur. Heart J.* **40**, 755–764 (2019).

4. Feigin, V. L. *et al.* Prevention of stroke: A strategic global imperative. *Nat. Rev. Neurol.* **12**, 501–512 (2016).

5. Valery L Feigin, Gregory A Roth, Mohsen Naghavi, Priya Parmar, Rita Krishnamurthi, S. C. DALYs : Results from the Global Burden of Disease Study 2013. *Lancet Neurol.* **45**, 203–214 (2016).

6. Virani, S. S. *et al.* Heart Disease and Stroke Statistics—2020 Update. *Circulation* **133**, 447–454 (2020).

7. Fisher, M. The ischemic penumbra: Identification, evolution and treatment concepts. *Cerebrovasc. Dis.* **17**, 1–6 (2004).

8. Hartings, J. A., Rolli, M. L., Lu, X. M. & Tortella, F. C. Delayed Hartings 2003 Secondary Phase of Peri-Infarct Depolarizations.pdf. **23**, 11602–11610 (2003).

9. Leao, A. A. P. Spreading Depression of Activity in the Cerebral Cortex. *J. Neurophysiol.* **7**, 359–390 (1944).

10. Somjen, G. G. Mechanisms of Spreading Depression and Hypoxic Spreading Depression-Like Depolarization. *Physiol. Rev.* **81**, 1065–1096 (2001).

11. Ayata, C. & Lauritzen, M. Spreading depression, spreading depolarizations, and the cerebral vasculature. *Physiol. Rev.* **95**, 953–993 (2015).

12. Dreier, J. P. The role of spreading depression, spreading depolarization and spreading ischemia in neurological disease. *Nat. Med.* **17**, 439–447 (2011).

13. Hoffmann, U. & Ayata, C. Neurovascular Coupling During Spreading Depolarizations. in *Cerebral Vasospasm: Neurovascular Events After Subarachnoid Hemorrhage* 161–165 (Springer Vienna, 2013). doi:10.1007/978-3-7091-1192-5_31.

14. Woitzik, J. *et al.* Propagation of cortical spreading depolarization in the human cortex after malignant stroke. *Neurology* **80**, 1095–1102 (2013).

15. Feuerstein, D. *et al.* Regulation of cerebral metabolism during cortical spreading depression. *J. Cereb. Blood Flow Metab.* **36**, 1965–1977 (2016).

16. Menyhárt, Á. *et al.* High incidence of adverse cerebral blood flow responses to spreading depolarization in the aged ischemic rat brain. *Neurobiol. Aging* **36**, 3269–3277 (2015).

17. Farkas, E., Obrenovitch, T. P., Institóris, Á. & Bari, F. Effects of early aging and cerebral hypoperfusion on spreading depression in rats. *Neurobiol. Aging* **32**, 1707–1715 (2011).

18. Tombaugh, G. C. Mild acidosis delays hypoxic spreading depression and improves neuronal

recovery in hippocampal slices. *J. Neurosci.* **14**, 5635–5643 (1994).

19. Jackman, K. & Iadecola, C. Neurovascular Regulation in the Ischemic Brain. *Antioxid. Redox Signal.* **22**, 149–160 (2015).

20. Menyhárt, Á. *et al.* Spreading depolarization remarkably exacerbates ischemia-induced tissue acidosis in the young and aged rat brain. *Sci. Rep.* **7**, 1–13 (2017).

21. Kuschinsky, W. & Wahl, M. Perivascular pH and pial arterial diameter during bicuculline induced seizures in cats. *Pflügers Arch. - Eur. J. Physiol.* **382**, 81–85 (1979).

22. Farkas, E. & Luiten, P. G. M. *Cerebral microvascular pathology in aging and Alzheimer's disease. Progress in Neurobiology* vol. 64 (2001).

23. Riddle, D. R., Sonntag, W. E. & Lichtenwalner, R. J. Microvascular plasticity in aging. *Ageing Res. Rev.* **2**, 149–168 (2003).

24. Bogorad, M. I., DeStefano, J. G., Linville, R. M., Wong, A. D. & Searson, P. C. Cerebrovascular plasticity: Processes that lead to changes in the architecture of brain microvessels. *J. Cereb. Blood Flow Metab.* **39**, 1413–1432 (2019).

25. Fulop, G. A. *et al.* Role of age-related alterations of the cerebral venous circulation in the pathogenesis of vascular cognitive impairment. *Am. J. Physiol. Circ. Physiol.* **316**, H1124–H1140 (2019).

26. Kalaria, R. N. & Hase, Y. Neurovascular Ageing and Age-Related Diseases. in 477–499 (2019). doi:10.1007/978-981-13-3681-2_17.

27. Riecker, A. *et al.* Relation between Regional Functional MRI Activation and Vascular Reactivity to Carbon Dioxide during Normal Aging. *J. Cereb. Blood Flow Metab.* **23**, 565–573 (2003).

28. Park, L., Anrather, J., Girouard, H., Zhou, P. & Iadecola, C. Nox2-Derived Reactive Oxygen Species Mediate Neurovascular Dysregulation in the Aging Mouse Brain. *J. Cereb. Blood Flow Metab.* **27**, 1908–1918 (2007).

29. Mayhan, W. G., Arrick, D. M., Sharpe, G. M. & Sun, H. Age-Related Alterations in Reactivity of Cerebral Arterioles: Role of Oxidative Stress. *Microcirculation* **15**, 225–236 (2008).

30. Toth, P. *et al.* Resveratrol treatment rescues neurovascular coupling in aged mice: role of improved cerebromicrovascular endothelial function and downregulation of NADPH oxidase. *Am. J. Physiol. Circ. Physiol.* **306**, H299–H308 (2014).

31. Balbi, M. *et al.* Dysfunction of Mouse Cerebral Arteries during Early Aging. *J. Cereb. Blood Flow Metab.* **35**, 1445–1453 (2015).

32. Lecrux, C. & Hamel, E. Neuronal networks and mediators of cortical neurovascular coupling responses in normal and altered brain states. *Philos. Trans. R. Soc. B Biol. Sci.* **371**, (2016).

33. Lecrux, C. *et al.* Impact of Altered Cholinergic Tones on the Neurovascular Coupling Response to Whisker Stimulation. *J. Neurosci.* **37**, 1518–1531 (2017).

34. Nizari, S., Carare, R. O., Romero, I. A. & Hawkes, C. A. 3D Reconstruction of the Neurovascular Unit Reveals Differential Loss of Cholinergic Innervation in the Cortex and Hippocampus of the Adult Mouse Brain. *Front. Aging Neurosci.* **11**, (2019).

35. Cai, W. *et al.* Dysfunction of the neurovascular unit in ischemic stroke and neurodegenerative diseases: An aging effect. *Ageing Res. Rev.* **34**, 77–87 (2017).

36. Erdő, F., Denes, L. & de Lange, E. Age-associated physiological and pathological changes at the blood–brain barrier: A review. *J. Cereb. Blood Flow Metab.* **37**, 4–24 (2017).

37. Osipova, E. D. *et al.* Designing in vitro Blood-Brain Barrier Models Reproducing Alterations in Brain Aging. *Front. Aging Neurosci.* **10**, (2018).

38. Di Marco, L. Y. *et al.* Vascular dysfunction in the pathogenesis of Alzheimer's disease — A review of endothelium-mediated mechanisms and ensuing vicious circles. *Neurobiol. Dis.* **82**, 593–606 (2015).

39. Toth, P., Tarantini, S., Csiszar, A. & Ungvari, Z. Functional vascular contributions to cognitive impairment and dementia: Mechanisms and consequences of cerebral autoregulatory dysfunction, endothelial impairment, and neurovascular uncoupling in aging. *Am. J. Physiol. - Hear. Circ. Physiol.* **312**, H1–H20 (2017).

40. Ay, H. *et al.* Conversion of Ischemic Brain Tissue Into Infarction Increases With Age. *Stroke* **36**, 2632–2636 (2005).

41. Popa-Wagner, A. *et al.* Accelerated infarct development, cytogenesis and apoptosis following transient cerebral ischemia in aged rats. *Acta Neuropathol.* **113**, 277–293 (2007).

42. Faber, J. E. *et al.* Aging Causes Collateral Rarefaction and Increased Severity of Ischemic Injury in Multiple Tissues. *Arterioscler. Thromb. Vasc. Biol.* **31**, 1748–1756 (2011).

43. Ma, J., Ma, Y., Shuaib, A. & Winship, I. R. Impaired Collateral Flow in Pial Arterioles of Aged Rats During Ischemic Stroke. *Transl. Stroke Res.* (2019) doi:10.1007/s12975-019-00710-1.

44. Zhang, H., Jin, B. & Faber, J. E. Mouse models of Alzheimer's disease cause rarefaction of pial collaterals and increased severity of ischemic stroke. *Angiogenesis* **22**, 263–279 (2019).

45. Lauritzen, M. Regional cerebral blood flow during cortical spreading depression in rat brain: increased reactive hyperperfusion in low-flow states. *Acta Neurol. Scand.* **75**, 1–8 (1987).

46. Hartings, J. A. *et al.* The continuum of spreading depolarizations in acute cortical lesion development: Examining Leão's legacy. *J. Cereb. Blood Flow Metab.* **37**, 1571–1594 (2017).

47. Farkas, E. & Bari, F. Spreading Depolarization in the Ischemic Brain: Does Aging Have an Impact? *Journals Gerontol. Ser. A Biol. Sci. Med. Sci.* **69**, 1363–1370 (2014).

48. Hertelendy, P., Varga, D. P., Menyhárt, Á., Bari, F. & Farkas, E. Susceptibility of the cerebral cortex to spreading depolarization in neurological disease states: The impact of aging. *Neurochem. Int.* **127**, 125–136 (2019).

49. Dreier, J. P. *et al.* Delayed ischaemic neurological deficits after subarachnoid haemorrhage are associated with clusters of spreading depolarizations. *Brain* **129**, 3224–3237 (2006).

50. Reinhart, K. M. & Shuttleworth, C. W. Ketamine reduces deleterious consequences of spreading depolarizations. *Exp. Neurol.* **305**, 121–128 (2018).

51. Szabó, Í. *et al.* The impact of dihydropyridine derivatives on the cerebral blood flow response to somatosensory stimulation and spreading depolarization. *Br. J. Pharmacol.* **176**, 1222–1234 (2019).

52. Lassen, N. A. Brain Extracellular pH: The Main Factor Controlling Cerebral Blood Flow. *Scand. J. Clin. Lab. Invest.* **22**, 247–251 (1968).

53. Siesjö, B. K., Kjällquist, Å., Pontén, U. & Zwetnow, N. Extracellular pH in the Brain and

Cerebral Blood Flow. in 93–98 (1968). doi:10.1016/S0079-6123(08)61444-2.

54. Clark, D. *et al.* Impact of aging on spreading depolarizations induced by focal brain ischemia in rats. *Neurobiol. Aging* **35**, 2803–2811 (2014).

55. Farkas, E., Pratt, R., Sengpiel, F. & Obrenovitch, T. P. Direct, Live Imaging of Cortical Spreading Depression and Anoxic Depolarisation Using a Fluorescent, Voltage-Sensitive Dye. *J. Cereb. Blood Flow Metab.* **28**, 251–262 (2008).

56. Farkas, E., Bari, F. & Obrenovitch, T. P. Multi-modal imaging of anoxic depolarization and hemodynamic changes induced by cardiac arrest in the rat cerebral cortex. *Neuroimage* **51**, 734–742 (2010).

57. Bere, Z., Obrenovitch, T. P., Kozák, G., Bari, F. & Farkas, E. Imaging Reveals the Focal Area of Spreading Depolarizations and a Variety of Hemodynamic Responses in a Rat Microembolic Stroke Model. *J. Cereb. Blood Flow Metab.* **34**, 1695–1705 (2014).

58. Domoki, F. *et al.* Evaluation of laser-speckle contrast image analysis techniques in the cortical microcirculation of piglets. *Microvasc. Res.* **83**, 311–317 (2012).

59. Obrenovitch, T. P., Chen, S. & Farkas, E. Simultaneous, live imaging of cortical spreading depression and associated cerebral blood flow changes, by combining voltage-sensitive dye and laser speckle contrast methods. *Neuroimage* **45**, 68–74 (2009).

60. Voipio, J. & Kaila, K. Interstitial PCO2 and pH in rat hippocampal slices measured by means of a novel fast CO2/H+-sensitive microelectrode based on a PVC-gelled membrane. *Pflügers Arch. Eur. J. Physiol.* **423**, 193–201 (1993).

61. Sonntag, W. E., Lynch, C. D., Cooney, P. T. & Hutchins, P. M. Decreases in cerebral microvasculature with age are associated with the decline in growth hormone and insulin-like growth factor 1. *Endocrinology* **138**, 3515–3520 (1997).

62. Brennan, K. C. *et al.* Distinct Vascular Conduction With Cortical Spreading Depression. *J. Neurophysiol.* **97**, 4143–4151 (2007).

63. Menyhárt, Á. *et al.* Large-conductance Ca2+-activated potassium channels are potently involved in the inverse neurovascular response to spreading depolarization. *Neurobiol. Dis.* **119**, 41–52 (2018).

64. Mayhan, W. G., Faraci, F. M., Baumbach, G. L. & Heistad, D. D. Effects of aging on responses of cerebral arterioles. *Am. J. Physiol. Circ. Physiol.* **258**, H1138–H1143 (1990).

65. Shatillo, A. *et al.* Cortical spreading depression induces oxidative stress in the trigeminal nociceptive system. *Neuroscience* **253**, 341–349 (2013).

66. Unekawa, M. *et al.* Dynamic diameter response of intraparenchymal penetrating arteries during cortical spreading depression and elimination of vasoreactivity to hypercapnia in anesthetized mice. *J. Cereb. Blood Flow Metab.* **37**, 657–670 (2017).

67. Girouard, H. & Iadecola, C. Neurovascular coupling in the normal brain and in hypertension, stroke, and Alzheimer disease. *J. Appl. Physiol.* **100**, 328–335 (2006).

68. Iadecola, C. The Neurovascular Unit Coming of Age: A Journey through Neurovascular Coupling in Health and Disease. *Neuron* **96**, 17–42 (2017).

69. Longden, T. A. *et al.* Capillary K+-sensing initiates retrograde hyperpolarization to increase local cerebral blood flow. *Nat. Neurosci.* **20**, 717–726 (2017).

70.   Bonnin, P., Mazighi, M., Charriaut-Marlangue, C. & Kubis, N. Early Collateral Recruitment After Stroke in Infants and Adults. *Stroke* **50**, 2604–2611 (2019).

71.   Wang, F. *et al.* Dysfunction of Cerebrovascular Endothelial Cells: Prelude to Vascular Dementia. *Front. Aging Neurosci.* **10**, (2018).

72.   Fordsmann, J. C. *et al.* Increased 20-HETE Synthesis Explains Reduced Cerebral Blood Flow But Not Impaired Neurovascular Coupling after Cortical Spreading Depression in Rat Cerebral Cortex. *J. Neurosci.* **33**, 2562–2570 (2013).

73.   Gariepy, H., Zhao, J. & Levy, D. Differential contribution of COX-1 and COX-2 derived prostanoids to cortical spreading depression—Evoked cerebral oligemia. *J. Cereb. Blood Flow Metab.* **37**, 1060–1068 (2017).

74.   Cipolla, M. J., Lessov, N., Hammer, E. S. & Curry, A. B. Threshold Duration of Ischemia for Myogenic Tone in Middle Cerebral Arteries. *Stroke* **32**, 1658–1664 (2001).

75.   Maneen, M. J. & Cipolla, M. J. Peroxynitrite diminishes myogenic tone in cerebral arteries: role of nitrotyrosine and F-actin. *Am. J. Physiol. Circ. Physiol.* **292**, H1042–H1050 (2007).

76.   Pundik, S., Xu, K. & Sundararajan, S. Reperfusion brain injury: Focus on cellular bioenergetics. *Neurology* **79**, S44–S51 (2012).

77.   Dreier, J. P. *et al.* Recording, analysis, and interpretation of spreading depolarizations in neurointensive care: Review and recommendations of the COSBID research group. *J. Cereb. Blood Flow Metab.* **37**, 1595–1625 (2017).

78.   Pinard, E., Nallet, H., MacKenzie, E. T., Seylaz, J. & Roussel, S. Penumbral Microcirculatory Changes Associated With Peri-infarct Depolarizations in the Rat. *Stroke* **33**, 606–612 (2002).

79.   Dreier, J. P. *et al.* Cortical spreading ischaemia is a novel process involved in ischaemic damage in patients with aneurysmal subarachnoid haemorrhage. *Brain* **132**, 1866–1881 (2009).

80.   Hartings, J. A. *et al.* Recovery of Slow Potentials in AC-Coupled Electrocorticography: Application to Spreading Depolarizations in Rat and Human Cerebral Cortex. *J. Neurophysiol.* **102**, 2563–2575 (2009).

81.   Pietrobon, D. & Moskowitz, M. A. Chaos and commotion in the wake of cortical spreading depression and spreading depolarizations. *Nat. Rev. Neurosci.* **15**, 379–393 (2014).

82.   Prince, D. A., Lux, H. D. & Neher, E. Measurement of extracellular potassium activity in cat cortex. *Brain Res.* **50**, 489–495 (1973).

83.   Mutch, W. A. C. & Hansen, A. J. Extracellular pH Changes during Spreading Depression and Cerebral Ischemia: Mechanisms of Brain pH Regulation. *J. Cereb. Blood Flow Metab.* **4**, 17–27 (1984).

84.   Scheller, D., Kolb, J. & Tegtmeier, F. Lactate and pH change in close correlation in the extracellular space of the rat brain during cortical spreading depression. *Neurosci. Lett.* **135**, 83–86 (1992).

85.   Menna, G., Tong, C. K. & Chesler, M. Extracellular pH Changes and Accompanying Cation Shifts During Ouabain-Induced Spreading Depression. *J. Neurophysiol.* **83**, 1338–1345 (2000).

86.   Tong, C. K. & Chesler, M. Modulation of Spreading Depression by Changes in Extracellular pH. *J. Neurophysiol.* **84**, 2449–2457 (2000).

87.   Chesler, M. & Kaila, K. Modulation of pH by neuronal activity. *Trends Neurosci.* **15**, 396–402

(1992).

88. Magnotta, V. A. *et al.* Detecting activity-evoked pH changes in human brain. *Proc. Natl. Acad. Sci.* **109**, 8270–8273 (2012).

89. Fox, P. T. & Raichle, M. E. Stimulus rate determines regional brain blood flow in striate cortex. *Ann. Neurol.* **17**, 303–305 (1985).

90. Hertelendy, P. *et al.* Advancing age and ischemia elevate the electric threshold to elicit spreading depolarization in the cerebral cortex of young adult rats. *J. Cereb. Blood Flow Metab.* **37**, 1763–1775 (2017).

91. Varga, D. P. *et al.* Contribution of prostanoid signaling to the evolution of spreading depolarization and the associated cerebral blood flow response. *Sci. Rep.* **6**, 1–10 (2016).

92. Cruz, N. F., Adachi, K. & Dienel, G. A. Rapid Efflux of Lactate from Cerebral Cortex during K + -Induced Spreading Cortical Depression. *J. Cereb. Blood Flow Metab.* **19**, 380–392 (1999).

93. Nedergaard, M., Goldman, S., Desai, S. & Pulsinelli, W. Acid-induced death in neurons and glia. *J. Neurosci.* **11**, 2489–2497 (1991).

94. Kraig, R. P., Petito, C. K., Plum, F. & Pulsinelli, W. A. Hydrogen Ions Kill Brain at Concentrations Reached in Ischemia. *J. Cereb. Blood Flow Metab.* **7**, 379–386 (1987).

95. Tang, C. M., Dichter, M. & Morad, M. Modulation of the N-methyl-D-aspartate channel by extracellular H+. *Proc. Natl. Acad. Sci.* **87**, 6445–6449 (1990).

96. Tombaugh, G. C. & Somjen, G. G. Effects of extracellular pH on voltage-gated Na+, K+ and Ca2+ currents in isolated rat CA1 neurons. *J. Physiol.* **493**, 719–732 (1996).

97. Benveniste, H., Drejer, J., Schousboe, A. & Diemer, N. H. Elevation of the Extracellular Concentrations of Glutamate and Aspartate in Rat Hippocampus During Transient Cerebral Ischemia Monitored by Intracerebral Microdialysis. *J. Neurochem.* **43**, 1369–1374 (1984).

98. Butcher, S. P., Bullock, R., Graham, D. I. & McCulloch, J. Correlation between amino acid release and neuropathologic outcome in rat brain following middle cerebral artery occlusion. *Stroke* **21**, 1727–1733 (1990).

99. Hernándéz-Cáceres, J., Macias-González, R., Brožek, G. & Bureš, J. Systemic ketamine blocks cortical spreading depression but does not delay the onset of terminal anoxic depolarization in rats. *Brain Res.* **437**, 360–364 (1987).

100. Harreveld, A. Van. COMPOUNDS IN BRAIN EXTRACTS CAUSING SPREADING DEPRESSION OF CEREBRAL CORTICAL ACTIVITY AND CONTRACTION OF CRUSTACEAN MUSCLE. *J. Neurochem.* **3**, 300–315 (1959).

101. Grafstein, B. MECHANISM OF SPREADING CORTICAL DEPRESSION. *J. Neurophysiol.* **19**, 154–171 (1956).

102. Hansen, A. J. The extracellular potassium concentration in brain cortex following ischemia in hypo- and hyperglycemic rats. *Acta Physiol. Scand.* **102**, 324–329 (1978).

103. Hansen, A. J. Effect of anoxia on ion distribution in the brain. *Physiol. Rev.* **65**, 101–148 (1985).

104. Selman, W. R., Lust, W. D., Pundik, S., Zhou, Y. & Ratcheson, R. A. Compromised metabolic recovery following spontaneous spreading depression in the penumbra. *Brain Res.* **999**, 167–

174 (2004).

105. Pierre, K. & Pellerin, L. Monocarboxylate transporters in the central nervous system: distribution, regulation and function. *J. Neurochem.* **94**, 1–14 (2005).

106. Drewes, L. R. & Gilboe, D. D. Glycolysis and the permeation of glucose and lactate in the isolated, perfused dog brain during anoxia and postanoxic recovery. *J. Biol. Chem.* **248**, 2489–2496 (1973).

107. Gerhart, D. Z., Enerson, B. E., Zhdankina, O. Y., Leino, R. L. & Drewes, L. R. Expression of monocarboxylate transporter MCT1 by brain endothelium and glia in adult and suckling rats. *Am. J. Physiol. Metab.* **273**, E207–E213 (1997).

108. Pellerin, L., Pellegri, G., Martin, J.-L. & Magistretti, P. J. Expression of monocarboxylate transporter mRNAs in mouse brain: Support for a distinct role of lactate as an energy substrate for the neonatal vs. adult brain. *Proc. Natl. Acad. Sci.* **95**, 3990–3995 (1998).